Comparative inverse analysis of satellite (MOPITT) and aircraft (TRACE-P) observations to estimate Asian sources of carbon monoxide

The Harvard community has made this article openly available. Please share how this access benefits you. Your story matters

Comparative inverse analysis of satellite (MOPITT) and aircraft (TRACE-P) observations to estimate Asian sources of carbon monoxide

Colette L. Heald,[1] Daniel J. Jacob,[1] Dylan B. A. Jones,[1,2] Paul I. Palmer,[1] Jennifer A. Logan,[1] D. G. Streets,[3] Glen W. Sachse,[4] John C. Gille,[5] Ross N. Hoffman,[6] and Thomas Nehrkorn[6]

[1]   We use an inverse model analysis to compare the top-down constraints on Asian sources of carbon monoxide (CO) in spring 2001 from (1) daily MOPITT satellite observations of CO columns over Asia and the neighboring oceans and (2) aircraft observations of CO concentrations in Asian outflow from the TRACE-P aircraft mission over the northwest Pacific. The inversion uses the maximum a posteriori method (MAP) and the GEOS-CHEM chemical transport model (CTM) as the forward model. Detailed error characterization is presented, including spatial correlation of the model transport error. Nighttime MOPITT observations appear to be biased and are excluded from the inverse analysis. We find that MOPITT and TRACE-P observations are independently consistent in the constraints that they provide on Asian CO sources, with the exception of southeast Asia for which the MOPITT observations support a more modest decrease in emissions than suggested by the aircraft observations. Our analysis indicates that the observations do not allow us to differentiate source types (i.e., anthropogenic versus biomass burning) within a region. MOPITT provides ten pieces of information to constrain the geographical distribution of CO sources, while TRACE-P provides only four. The greater information from MOPITT reflects its ability to observe all outflow and source regions. We conducted a number of sensitivity studies for the inverse model analysis using the MOPITT data. Temporal averaging of the MOPITT data (weekly and beyond) degrades the ability to constrain regional sources. Merging source regions beyond what is appropriate after careful selection of the state vector leads to significant aggregation errors. Calculations for an ensemble of realistic assumptions lead to a range of inverse model solutions that has greater uncertainty than the a posteriori errors for the MAP solution. Our best estimate of total Asian CO sources is 361 Tg yr^{-1}, over half of which is attributed to east Asia.   *INDEX TERMS:* 0322 Atmospheric Composition and Structure: Constituent sources and sinks; 0365 Atmospheric Composition and Structure: Troposphere—composition and chemistry; 0368 Atmospheric Composition and Structure: Troposphere—constituent transport and chemistry; *KEYWORDS:* MOPITT, TRACE-P, carbon monoxide, Asia, Bayesian synthesis, inversion

1. Introduction

[2]   Observations of atmospheric trace species from satellite and aircraft provide "top-down" constraints for quantifying emissions to the atmosphere. These can help to improve the traditional "bottom-up" emission estimates that apply emission factors to socioeconomic, energy, land use or environmental data. Bayesian inverse methods provide a formal basis for obtaining optimized emission estimates from the combination of top-down and bottom-up constraints. A forward model, in our case the GEOS-CHEM chemical transport model (CTM), provides the connection between emissions and species concentrations in the atmosphere. Most applications of inverse methods so

---

[1]Department of Earth and Planetary Sciences and Division of Engineering and Applied Sciences, Harvard University, Cambridge, Massachusetts, USA.

[2]Now at Department of Physics, University of Toronto, Toronto, Ontario, Canada.

[3]Argonne National Laboratory, Argonne, Illinois, USA.

[4]NASA Langley Research Center, Hampton, Virginia, USA.

[5]National Center of Atmospheric Research, Boulder, Colorado, USA.

[6]AER Inc., Lexington, Massachusetts, USA.

far have used observational constraints from surface stations; for carbon monoxide (CO) emissions these include *Bergamaschi et al.* [2000], *Kasibhatla et al.* [2002], and *Pétron et al.* [2002]. Two recent studies for CO have exploited the high density of observational coverage from aircraft [*Palmer et al.*, 2003a] and satellites [*Arellano et al.*, 2004]. As satellite observations of atmospheric composition become increasingly available one should examine their value for constraining emissions and their complementarity with in situ observations. We address this issue here with a comparative inverse model analysis of satellite (MOPITT) and aircraft (TRACE-P) observations aimed at quantifying Asian sources of CO.

[3] Carbon monoxide is a tracer of pollution and the primary sink of hydroxyl (OH), the main tropospheric oxidant. It is emitted by incomplete combustion and is also produced within the atmosphere by oxidation of methane and volatile organic compounds (VOCs). It is removed from the atmosphere by oxidation by OH with a lifetime of a few months. Quantifying Asian sources of combustion gases including CO is of considerable interest as these sources represent a substantial global perturbation to atmospheric composition [*Berntsen et al.*, 1996] and are expected to be the principal driver of global atmospheric change over the coming decades [*IPCC*, 2001].

[4] Asian chemical outflow was extensively sampled from the surface to 12 km altitude during the NASA Transport and Chemical Evolution over the Pacific (TRACE-P) aircraft mission in March–April 2001 [*Jacob et al.*, 2003]. The Measurement of Pollution in the Troposphere (MOPITT) satellite instrument [*Drummond and Mand*, 1996; *Edwards et al.*, 1999] was simultaneously measuring CO aboard the EOS-Terra polar-orbiting platform. A detailed bottom-up anthropogenic emission inventory for east Asia in 2000 was developed by *Streets et al.* [2003] in support of TRACE-P. Bottom-up emission estimates for biomass burning, a major CO source in southeast Asia in that season, were also derived by applying daily satellite fire count data to climatological emission inventories [*Heald et al.*, 2003a; *Woo et al.*, 2003].

[5] *Palmer et al.* [2003a], the forerunner for this work, presented an inverse model analysis of Asian CO sources using exclusively the TRACE-P aircraft observations as top-down constraints and the bottom-up inventories of *Streets et al.* [2003] (anthropogenic) and *Heald et al.* [2003a] (biomass burning) as a priori bottom-up constraints. They used the GEOS-CHEM CTM as the forward model, as we do here. They found that anthropogenic sources in China in the *Streets et al.* [2003] inventory were underestimated by 54%, whereas biomass burning sources in SE Asia in the *Heald et al.* [2003a] inventory were too high by a factor of three. Another study by *Allen et al.* [2004] used the TRACE-P observations to constrain Asian anthropogenic and biomass burning CO sources by linear regression of their CTM simulation against observations. They obtained continental-scale estimates of Asian sources consistent with those derived by *Palmer et al.* [2003a], and further showed that these optimized sources afford a good simulation of the MOPITT observations.

[6] We apply here a Bayesian inverse model analysis to investigate the top-down constraints on Asian sources

provided by the daily MOPITT observations for the TRACE-P period, and to compare to the constraints provided by the TRACE-P aircraft observations. Our first focus is to determine if the constraints from satellite and aircraft are consistent, and if so whether they are complementary or redundant. Our second focus is to better understand how to use satellite observations such as MOPITT in inverse modeling of sources. The latter will lead us into discussions of observational error covariances, temporal resolution in the satellite data, and ensemble modeling versus Bayesian statistics.

2. Data and Methods

[7] We use both MOPITT satellite and TRACE-P aircraft observations to constrain Asian CO sources using an inverse model analysis. We first present the inverse methodology (section 2.1), and go on to briefly describe the observations (section 2.2), the a priori emissions (section 2.3) and the forward model (section 2.4). Error characterization is described in section 3.

2.1. Inverse Model Methodology

[8] The inverse method seeks an optimal solution for Asian sources of CO consistent with both the observed atmospheric concentrations and the a priori bottom-up constraints. These sources are partitioned geographically or by source type as discussed in section 4. We assume that their spatial and temporal patterns (as defined by energy use and fire count data) are correct and solve for their amplitudes. We arrange the source amplitudes to be optimized into a state vector $\mathbf{x}$ of dimension n, and the ensemble of observed concentrations to be used in the optimization into an observation vector $\mathbf{y}$ of dimension q. We relate $\mathbf{x}$ to $\mathbf{y}$ by:

$$\mathbf{y} = \mathbf{Kx} + \varepsilon_\Sigma \quad (1)$$

Here the Jacobian ($\mathbf{K}$) represents the linear CTM used to relate sources to concentrations in a forward sense (forward model). The linear approximation will be discussed in section 2.4. The total (Σ) observational error (ε_Σ) includes contributions from CTM error, representation error (sampling mismatch between the observations and the model), and measurement error. Assuming the errors are unbiased and normally distributed, the characteristics of these errors are described by the error covariance matrix of the system ($\mathbf{S}_\Sigma$). The bottom-up CO source estimates (section 2.3) represent the a priori knowledge of the state vector ($\mathbf{x}_a$).

[9] The solution to the inverse problem consists of minimizing a χ^2 scalar-valued cost function $J(\mathbf{x})$ [*Rodgers*, 2000]:

$$J(\mathbf{x}) = (\mathbf{y} - \mathbf{Kx})^\mathbf{T}\mathbf{S}_\Sigma^{-1}(\mathbf{y} - \mathbf{Kx}) + (\mathbf{x} - \mathbf{x}_a)^\mathbf{T}\mathbf{S}_a^{-1}(\mathbf{x} - \mathbf{x}_a) \quad (2)$$

The first term on the right hand side of equation (2) represents the mismatch between simulated and observed concentrations weighted by the error covariance of the system. The second term represents the departure of the true value $\mathbf{x}$ of the state vector from the a priori estimate $\mathbf{x}_a$, weighted by the error covariance of the a priori state vector ($\mathbf{S}_a$). The resulting maximum a posteriori (MAP) solution
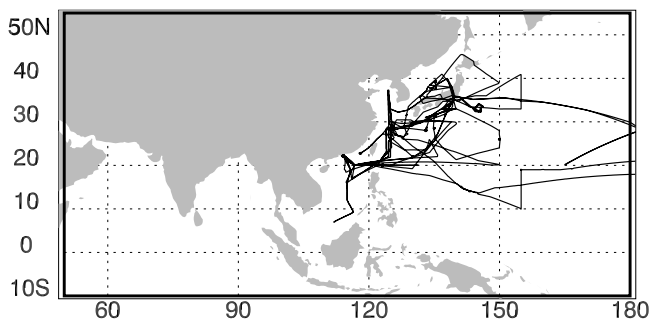
Figure 1. Geographical domain of the MOPITT observations used in the analysis. TRACE-P flight tracks are also shown.

for the state vector ($\hat{\mathbf{x}}$) and its associated error covariance ($\hat{\mathbf{S}}$) is [*Rodgers*, 2000]:

$$\hat{\mathbf{x}} = \mathbf{x}_a + \mathbf{S}_a \mathbf{K}^{\mathbf{T}} \left(\mathbf{K} \mathbf{S}_a \mathbf{K}^{\mathbf{T}} + \mathbf{S}_\Sigma \right)^{-1} (\mathbf{y} - \mathbf{K} \mathbf{x}_a) \qquad (3)$$

$$\hat{\mathbf{S}}^{-1} = \mathbf{K}^{\mathbf{T}} \mathbf{S}_\Sigma^{-1} \mathbf{K} + \mathbf{S}_a^{-1} \qquad (4)$$

[10] Equations (3) and (4) can be applied sequentially to subsets of observations by using $\hat{\mathbf{x}}$ and $\hat{\mathbf{S}}$ as $\mathbf{x}_a$ and $\mathbf{S}_a$ for the next subset. This avoids the multiplication and inversion of very large matrices, and does not modify the results as long as the observational errors across different subsets are uncorrelated [*Rodgers*, 2000]. We assume that this is the case for data collected on separate days and thus apply equations (3) and (4) successively to each day of observations in order to obtain the MAP solution. Error correlation in data for individual days is described in section 3.
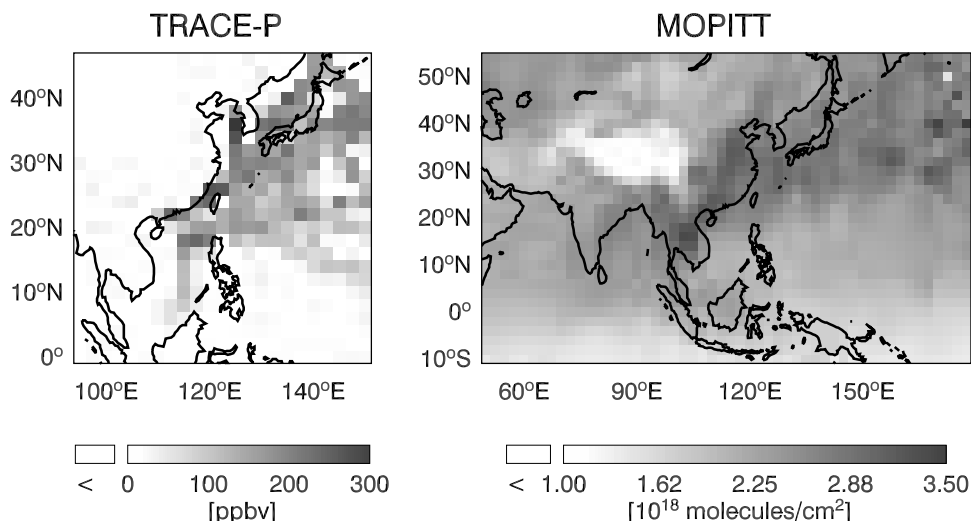
2.2. Observations

2.2.1. TRACE-P

[11] The TRACE-P aircraft mission aimed to characterize the chemical outflow from Asia and relate it quantitatively to its sources [*Jacob et al.*, 2003]. It was conducted from 26 February to 9 April 2001. Two aircraft extensively sampled Asian outflow up to 12 km altitude over the western Pacific from bases in Hong Kong and Japan. Flight tracks are shown in Figure 1. Asian outflow was driven by midlatitude cyclones originating over northeastern Asia and the associated cold fronts sweeping through east Asia [*Fuelberg et al.*, 2003]. Pollution was lifted in the warm conveyor belts (WCBs) ahead of the fronts, and was also advected to the Pacific in the boundary layer outflow behind the fronts [*Hannan et al.*, 2003; *Liu et al.*, 2003; *Miyazaki et al.*, 2003]. Deep convection was an additional boundary layer ventilating mechanism for southeast Asia [*Liu et al.*, 2003].

[12] Observations of CO on both aircraft were made continuously using the Differential Absorption of CO Measurement (DACOM) instrument [*Sachse et al.*, 1987]. These observations have a 1-s precision of 1% and a 1-min accuracy of 2%. We average the data for individual flights over the CTM grid ($2° \times 2.5°$ horizontal, ~1 km vertical) corresponding to a 20-min sampling interval at typical aircraft speeds (Figure 2). We remove stratospheric data as diagnosed by $O_3 > 100$ ppb in this averaged data set (we checked that this criterion does not eliminate any pollution plumes) and use only data west of 150°E (effectively eliminating the sparse data from transit flights).

2.2.2. MOPITT

[13] The MOPITT instrument is a nadir IR correlation radiometer launched in 1999 aboard the NASA Terra satellite [*Drummond and Mand*, 1996; *Edwards et al.*, 1999]. The satellite is in a polar Sun-synchronous orbit with a 1030 local time (LT) northward or southward local equator cross-over time. The instrument field of view is 22×22 km^2. Cross-track scanning with a 612 km swath provides global coverage approximately every 3 days. CO columns and profiles are retrieved from the IR emission channels (4.6 μm) for all cloud-free scenes [*Deeter et al.*, 2003]. We use daily CO version 3 data (http://www.eos.ucar.edu/mopitt/) for spring of 2001 over the Asian domain (10°S–55°N, 50–180°E) shown in Figure 1.

Figure 2. Mean CO observations during the TRACE-P mission (26 February to 9 April 2001) averaged over the $2° \times 2.5°$ grid of the GEOS-CHEM CTM. TRACE-P aircraft concentrations averaged over all altitudes are shown on the left. The MOPITT CO columns (morning overpasses only) are shown on the right. See color version of this figure at back of this issue.

[14] The MOPITT retrievals are performed with the maximum a posteriori method [*Rodgers*, 2000], similar to the method used here for inverse modeling (section 2.1). The state vector for the MOPITT retrieval includes the vertical profile **z** of CO concentrations, as well as ancillary surface properties. The observations are the measured radiances [*Deeter et al.*, 2003]. The a priori ($\mathbf{z}_a$) is a CO profile that decreases from 120 ppb at the surface to less than 60 ppb above 150 hPa, as obtained by averaging aircraft observations from a number of field campaigns; the covariance of these observations defines the error covariance matrix $\mathbf{S}_{za}$ on the a priori [*Deeter et al.*, 2003].

[15] To compare actual CO profiles to those retrieved from MOPITT it is necessary to simulate the retrieval by applying the MOPITT averaging kernel matrix ($\mathbf{A}_{zz}$), which describes the vertical smoothing of the profile. MOPITT averaging kernels show peak sensitivity in the middle and upper troposphere and low sensitivity in the boundary layer [*Deeter et al.*, 2003]. We compute them for individual retrievals from the a posteriori error covariance matrix ($\hat{\mathbf{S}}_z$) provided in the standard MOPITT product with each vertical profile:

$$\mathbf{A}_{zz} = \mathbf{I} - \hat{\mathbf{S}}_z \mathbf{S}_{za}^{-1} \tag{5}$$

The retrieval of the MOPITT CO profile ($\hat{\mathbf{z}}$) on 7 pressure levels (surface, 850, 700, 500, 350, 250, and 150 hPa) is related to the true concentration profile (**z**) by:

$$\hat{\mathbf{z}} = \mathbf{z}_a + \mathbf{A}_{zz}(\mathbf{z} - \mathbf{z}_a) + \mathbf{G}_z \boldsymbol{\varepsilon}_z \tag{6}$$

The last term in equation (6) describes the contribution of the total measurement error ($\boldsymbol{\varepsilon}_z$) (including radiative transfer forward model error, model parameter error, and instrument noise), multiplied by a gain matrix ($\mathbf{G}_z$). See *Rodgers* [2000] for the derivation of equations (5) and (6).

[16] MOPITT information of CO concentrations at the 7 pressure levels of a given vertical profile is highly correlated; the number of independent pieces of information in the vertical profile is generally less than 1.5 [*Heald et al.*, 2003b]. Therefore we only use CO column. We obtain the CO column $\hat{c}$ and associated error variance $\hat{S}_c$ by integrating the profile over the depth of the atmosphere:

$$\hat{c} = \mathbf{t}^{\mathbf{T}} \hat{\mathbf{z}} \tag{7}$$

$$\hat{S}_c = \mathbf{t}^{\mathbf{T}} \hat{\mathbf{S}}_z \mathbf{t} \tag{8}$$

where **t** is a transfer operator that includes both the conversion from volume mixing ratio to number density and the vertical integration in the pressure coordinate. MOPITT CO column validation with numerous in situ aircraft profiles indicates a positive bias of $4.9 \pm 10.8\%$ [*Emmons et al.*, 2004]. Validation during TRACE-P for four coincident MOPITT overpasses indicates a high correlation between MOPITT and aircraft columns, and a MOPITT positive bias of $6 \pm 2\%$ [*Jacob et al.*, 2003]. For purpose of the inverse analysis we average the MOPITT columns over the $2° \times 2.5°$ GEOS-CHEM model grid (Figure 2).

2.3. A Priori Sources

[17] Our a priori sources of CO for east Asia include a year 2000 regional inventory of fossil fuel and biofuel emissions [*Streets et al.*, 2003] and a daily biomass burning emission inventory constrained with satellite fire counts [*Heald et al.*, 2003a]. Fossil fuel, biofuel, and biomass burning emissions for the rest of the world are taken from B. N. Duncan (Model study of the variability and trends of carbon monoxide (1988–1997): 1. Model formulation, evaluation, and sensitivity, submitted to *Journal of Geophysical Research*, 2004, hereinafter referred to as Duncan et al., submitted manuscript, 2004), *Yevich and Logan* [2003], and *Duncan et al.* [2003], respectively. All inventories are available with $1° \times 1°$ horizontal resolution. A regional break-down of these combustion sources (including atmospheric production from oxidation of anthropogenic VOCs as described below) is in Table 1. Although our observational constraints (MOPITT and TRACE-P) are for spring only, we use yearly emissions as source amplitudes in our definition of the state vector. This effectively assumes that the seasonal scaling factor from spring to annual is known. Anthropogenic sources in Asia in spring match the annual average [*Streets et al.*, 2003].

[18] The chemical source of CO from the oxidation of methane and nonmethane volatile organic compounds (NMVOCs) is treated following the approach of Duncan et al. (submitted manuscript, 2004), with the exception of the isoprene oxidation source where a constant 30% yield per carbon atom is assumed. Nonbiogenic NMVOC emissions are generally coemitted with CO, and are therefore modeled by increasing primary CO emissions by 19% and 16% for anthropogenic emissions and biomass burning emissions respectively. The CO sources from oxidation of methane (850 Tg yr^{-1}), isoprene (187 Tg yr^{-1}), monoterpenes (70 Tg yr^{-1}), methanol (68 Tg yr^{-1}), and acetone (30 Tg yr^{-1}) are grouped into a separate component of the state vector (Table 1).

[19] The errors on the a priori sources (diagonal terms of $\mathbf{S}_a$) for the anthropogenic sectors in Asia were estimated by *Streets et al.* [2003] by propagation of uncertainties in the construction of their bottom-up inventories. We use their values and cap them at 100% (Table 1). Following *Palmer et al.* [2003a], we assume the uncertainty on the biomass burning source to be 50%. The uncertainty on anthropogenic sources outside of Asia is assumed to be 30% for North America and Europe, and 50% for the rest of the world. A 25% uncertainty is assigned to the source from oxidation of methane and biogenic NMVOCs on the basis of uncertainty on the global mean OH concentration [*Palmer et al.*, 2003a]. These various errors are assumed to be uncorrelated so that the resulting matrix $\mathbf{S}_a$ is diagonal.

2.4. Forward Model

[20] The forward model is the GEOS-CHEM CTM v.4.33 (http://www-as.harvard.edu/chemistry/trop/geos/index.html) applied to a CO-only simulation for spring of 2001 with specified OH concentration fields. We use the same model version as *Palmer et al.* [2003a] to facilitate comparison. The simulation is driven by assimilated meteorological data with a temporal resolution of 6 hours (3 hours for surface variables and mixing depths) from the Goddard Earth Observing System (GEOS)-3 of the NASA Global Modeling and Assimilation Office (GMAO). The GEOS-3 data for 2001 have a horizontal resolution of $1° \times 1°$ with 48 levels in the vertical; for input to GEOS-CHEM we degrade the

Table 1. Sources of CO Constrained in the Inverse Model Analysis[a]

TRACE-P State Vector[b]	MOPITT State Vector[b]	Region	A Priori Sources, Tg yr^{-1}			Uncertainty on A Priori Sources, %			A Posteriori Sources,[c] Tg yr^{-1}	Ratio[d]
			Fossil Fuel[e]	Biofuel[e]	Biomass burning[e]	Total	Fossil Fuel and Biofuels	Biomass Burning		
1	1	Japan (Jp)	5.1	2.0	0.7	**7.7**	17	50	37.5	2.67
		Korea (Ko)	3.4	2.8	0.1	**6.3**	42	50		
	2	N. China (ChNE)	2.5	3.0	2.4	**7.8**	78	50	2.5	0.32
2	3	C. China (ChCE)	26.4	14.0	1.3	**41.6**	78	50	61.4	1.48
	4	W. China (ChW)	12.9	12.6	4.7	**30.1**	78	50	63.9	2.12
3	5	S. China (ChSE)	17.5	12.5	0.3	**30.3**	78	50	26.3	0.87
4	6	SE Asia (SEAs)	6.7	13.1	49.3	**69.2**	100	50	42.0	0.61
5	7	Philippines (Ph)	0.5	1.1	3.9	**5.6**	100	50	2.7	0.48
6	8	Indonesia (Id)	5.0	13.7	36.9	**55.6**	100	50	78.4	1.41
	9	India (In)	14.3	36.9	38.7	**89.9**	100	50	45.8	0.51
	10	Europe (EU)	100	21.1	23.7	**145**	30	50	105	0.73
	11	rest of world (RoW)	183	67.3	346	**596**	50	50	2069	1.15
		methane and biogenic NMVOCs				**1205**	25			
		Total	**377**	**200**	**508**	**2291**			**2535**	1.08
		Asian total[f]	**94**	**112**	**138**	**344**			**361**	1.05

[a]See Figure 1 for geographical definition of the source regions.
[b]State vectors of sources constrained by the TRACE-P observations (6 elements) and the MOPITT observations (11 elements).
[c]Results from our best case inverse model analysis using daily, daytime-only MOPITT data for the TRACE-P period, and including spatial-correlation structure in the observational error (NMC method).
[d]Ratio of a posteriori to a priori sources for the 11 elements of the MOPITT-based state vector.
[e]Including both direct emission and atmospheric production from oxidation of combustion NMVOCs (section 2.3).
[f]Asia defined as regions numbered 1−9 in the MOPITT-based state vector.

horizontal resolution to 2° latitude by 2.5° longitude. The simulation is initialized in January 2000 and spun up through January 2001 to achieve proper initialization.

[21] We use archived monthly mean OH concentration fields from a previous O$_3$-NO$_x$-NMVOC simulation for 2001 [*Fiore et al.*, 2003]. Our global annual mean pressure-weighted OH concentration below 200 hPa is 1.00×10^6 cm^{-3}, which can be compared to estimates of $(0.94 \pm 0.13) \times 10^6$ cm^{-3} [*Prinn et al.*, 2001] and $1.07^{+0.09}_{-0.17} \times 10^6$ cm^{-3} [*Krol et al.*, 1998] based on observations of methylchloroform.

[22] The GEOS-CHEM CTM has previously been applied in a number of TRACE-P studies demonstrating a good simulation of Asian outflow [*Heald et al.*, 2003b; *Jaeglé et al.*, 2003; *Kiley et al.*, 2003; *Li et al.*, 2003; *Liu et al.*, 2003; *Palmer et al.*, 2003a, 2003b; *Suntharalingam et al.*, 2004; *Xiao et al.*, 2004]. GEOS-CHEM model forecasts were conducted in support of the TRACE-P mission and showed no transport bias except possibly in the upper troposphere (I. Bey et al., Characterization of transport errors in chemical forecasts from a global tropospheric chemical transport model, submitted to *Journal of Geophysical Research*, 2004, hereinafter referred to as Bey et al., submitted manuscript, 2004). Data from these forecasts will be employed here to determine the spatial covariance structure of the CTM transport error (see section 3.3).

[23] We use the forward model to construct the Jacobian matrix **K** (section 2.1) which describes the expected sensitivity of the observed concentrations to the individual state vector components (CO sources from a given region). Assuming a fixed OH concentration effectively linearizes the inverse problem, such that the methods in section 2.1 can be applied [*Pétron et al.*, 2002]. Nonlinearity is not a significant issue here since the observations used to constrain Asian sources are only a few days downwind of the Asian continent while the lifetime of CO is a few

months. Nonlinearity in the MOPITT retrieval is also negligible (D. Edwards, personal communication, 2003).

[24] In the case of the MOPITT inversion, the observations defining the rows of the Jacobian matrix are the CO columns smoothed by the MOPITT averaging kernels. For a given day, a model 2° × 2.5° grid square may encompass several MOPITT 22 × 22 km^2 observations, each with a different averaging kernel. The GEOS-CHEM profile for each individual MOPITT scene is smoothed through the corresponding MOPITT averaging kernel by applying equation (6) with $\varepsilon_z = 0$. The resulting smoothed model profiles, re-gridded to the 2° × 2.5° resolution of GEOS-CHEM, are used as the forward model simulation of the MOPITT observations.

[25] We construct the Jacobian by "tagging" as separate tracers in the CTM the contribution from each source region (Figure 3) to the CO concentration fields for the location and time of the observations. Each column of the Jacobian corresponds to a given state vector element and is obtained from the forward simulation as the ensemble of the corresponding tagged concentrations for a source of unit amplitude.

3. Characterization of the Observational Error

[26] Proper characterization of the observational error, as described by the error covariance matrix **S**$_\Sigma$ in equations (3) and (4), is crucial to the MAP solution of the inverse problem. **S**$_\Sigma$ can be decomposed into a sum of error covariance matrices describing the instrument error (**S**$_I$), the representation error (**S**$_R$), and the forward model error (**S**$_M$):

$$\mathbf{S}_\Sigma = \mathbf{S}_I + \mathbf{S}_R + \mathbf{S}_M \qquad (9)$$

Instrument and representation errors are assumed to be uncorrelated across the different observations, so that **S**$_I$ and
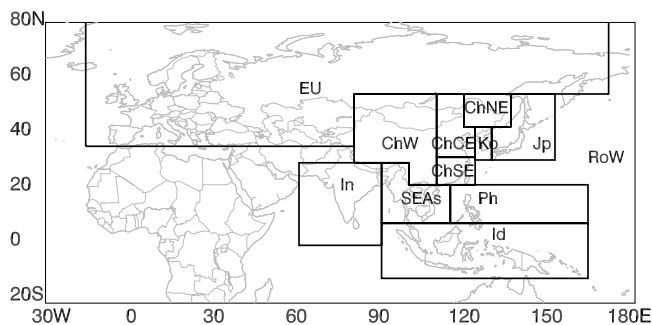
Figure 3. CO source regions used to define the state vector of the inverse model (Table 1).

$\mathbf{S}_R$ are diagonal. The forward model error has a covariance structure which we discuss in section 3.3. For now we focus on the diagonal structure of $\mathbf{S}_\Sigma$, representing the error variances for the individual observations.

[27] The dimension of $\mathbf{S}_\Sigma$ is that of the observation vector **y** used in the inversion. Each observation element of **y** is a spatial average over the $2° \times 2.5°$ CTM grid collected within a 3-hour time window. For MOPITT it is a column concentration, obtained by applying the column operator (**t**) to the retrieved 7-component vertical profile, while for TRACE-P it is a volume concentration. We assume that errors on observations taken on separate days are uncorrelated and apply the inverse model calculation on successive days as a sequential update algorithm (section 2.1). The dimension of $\mathbf{S}_\Sigma$ is then that of the ensemble of observations for a given day, which keeps the matrix operations computationally tractable. What follows in this section are the details of the error specification for the inverse analysis, it can be skipped by readers primarily interested in the resulting CO source estimates.

3.1. Calculating the Observational Error Variance

[28] We use the relative residual error (RRE) method of *Palmer et al.* [2003a] to estimate the variance of the observational error. In this method, we first compute statistics of the difference between the observed concentrations and those simulated by GEOS-CHEM using a priori sources. The mean value of this difference for the ensemble of observations (or a subset of that ensemble, see below) describes the model bias and is assumed to be due to error on the a priori sources. The residual is taken to represent the observational error. *Palmer et al.* [2003a] took the residual to represent only the forward model error, but as we show below it also includes contributions from instrument and representation errors, and thus it should be viewed as the total observational error. This distinction makes little difference in our application or the *Palmer et al.* [2003a] work since instrument and representation errors are small (section 3.2).

[29] Application of the RRE method is as follows. We partition the observation vector into subsets within which the error statistics are assumed to be homogeneous. For TRACE-P it is partitioned by altitude and latitude [*Palmer et al.*, 2003a], while for MOPITT it is partitioned as time series for the individual $2° \times 2.5°$ model grid squares. Let y_o be an element of the observation vector **y**, i.e., a single

observation, let y_M be the corresponding concentration simulated by GEOS-CHEM with a priori sources, and let y be the true concentration at that observation point. We have

$$y_o = y + \varepsilon_I \qquad (10)$$

where ε_I is the instrument error, and

$$y_M = y + b + \varepsilon_M + \varepsilon_R \qquad (11)$$

where ε_M is the forward model error and ε_R is the representation error. The model bias $b = \overline{y_M - y}$ is the mean model error for the ensemble of observation points in the subset (the overbar is the averaging operator). We calculate it as $b = \overline{y_M - y_o}$, which is a good approximation for a sufficiently large ensemble of observations since ε_I, ε_R, ε_M have mean values of zero. Thus the difference between observed and simulated concentrations (equations (10) and (11)) leads to an expression for the total observational error (ε_Σ):

$$\varepsilon_\Sigma = y_M - y_o - b \qquad (12)$$

with

$$\varepsilon_\Sigma = \varepsilon_I + \varepsilon_R + \varepsilon_M \qquad (13)$$

where we have reversed the sign of ε_I for the purpose of writing equation (13).

[30] We compile statistics of ε_Σ from application of equation (12) to all observation elements within a data subset and obtain in this manner the standard deviation of the residual error (σ_Σ). We divide it by the mean observed concentration $\overline{y_o}$ for the subset to define a relative residual standard deviation (RRSD). Finally, for each individual observation y_o we calculate the observational error variance as $(RRSD * y_o)^2$, and this value represents the corresponding diagonal element of $\mathbf{S}_\Sigma$. *Palmer et al.* [2003a] calculated values of 20–30% for the RRSD in the TRACE-P data in 1 km altitude intervals and in two latitude bands, and we use those values here for the TRACE-P data inversion.

[31] For the MOPITT column data we calculate model versus observed difference statistics for the time series for individual $2° \times 2.5°$ grid squares, using the ensemble of observations collected from 26 February to 9 April 2001 (the TRACE-P period), and smoothing the model fields through the corresponding averaging kernels ($\mathbf{A}_{zz}$) in order to compare to observations. The resulting observational error statistics, expressed as RRSD, are shown in Figure 4. Errors range from 5 to 30% and are highest over source regions with active convective transport, such as SE Asia. In principle one could construct the full observational error covariance matrix by examining the covariance of the model versus observed difference between different grid squares, but the TRACE-P and even the MOPITT data are too sparse for this purpose. We use a different approach, described in section 3.3, to determine the spatial correlation of the observational errors.

3.2. Contributions to Observational Error

[32] One can decompose the total observational error into contributions from instrument, representation, and forward
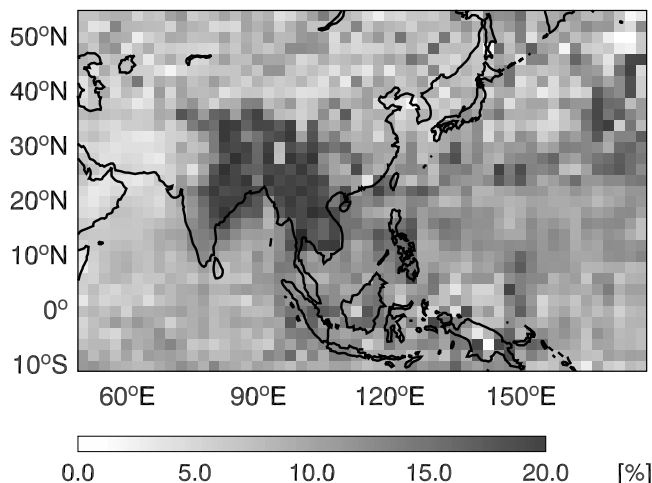
Figure 4. Total observational error variance (diagonal elements of $\mathbf{S}_\Sigma$) for the MOPITT data using GEOS-CHEM as forward model (morning overpasses only). See color version of this figure at back of this issue.

model errors (equation (9)). The instrument error for the TRACE-P aircraft data is negligibly small (section 2.2.1). For MOPITT the retrieval error covariance $(\hat{\mathbf{S}}_z)$ of a given profile reflects the uncertainty on the estimate of the true profile of CO and includes contributions from the vertical smoothing of the measurement (described by the averaging kernel $\mathbf{A}_{zz}$ of equation (5)) and the actual instrument measurement error covariance $(\mathbf{S}_\varepsilon)$ amplified by processing through the radiative transfer model [Rodgers, 2000]:

$$\hat{\mathbf{S}}_z = (\mathbf{A}_{zz} - \mathbf{I})\mathbf{S}_z(\mathbf{A}_{zz} - \mathbf{I})^\mathbf{T} + \mathbf{G}_z\mathbf{S}_\varepsilon\mathbf{G}_z^\mathbf{T} \qquad (14)$$

where $\mathbf{S}_z$ is the covariance of CO concentrations in the true atmosphere. We assume that the covariance on the a priori used in the MOPITT retrieval $(\mathbf{S}_{za})$ [Deeter et al., 2003] can be used to approximate this covariance, that is $\mathbf{S}_z = \mathbf{S}_{za}$. The gain matrix $(\mathbf{G}_z)$ converts from radiances to CO concentrations by inversion of the radiative transfer model.

[33] We find that the retrieval error is generally 5–15% and is dominated by the smoothing term, as shown previously in descriptions of the MOPITT retrieval algorithm [Pan et al., 1998; Wang et al., 1999]. However, since we also smooth the model profiles with the MOPITT averaging kernels, we must remove that contribution from the instrument error. The instrument error covariance for a single profile $(\mathbf{S}_i)$ therefore consists solely of the uncertainty associated with the instrument and the radiative transfer model:

$$\mathbf{S}_i = \mathbf{G}_z\mathbf{S}_\varepsilon\mathbf{G}_z^\mathbf{T} \qquad (15)$$

We apply the column transfer operator $(\mathbf{t})$ to calculate the corresponding error variance on the column concentration, $\mathbf{t}^T\mathbf{S}_i\mathbf{t}$, representing a diagonal element of $\mathbf{S}_I$. We find that this error is small, in the range of 1–3% of the CO column for our domain of interest.

[34] The representation error (covariance matrix $\mathbf{S}_R$) describes the mismatch in space and time between the measurements and the corresponding values simulated by the forward model. This error arises because the model only provides concentration data averaged over the $2° \times 2.5°$ grid scale and every 3 hours, but the observations do not fully cover that scale and may also be displaced by up to 1.5 hours. Palmer et al. [2003a] previously estimated this error in their inversion of the TRACE-P data by examining the variability of aircraft observations (1-min averages) over the model grid ($2° \times 2.5°$). Typical values were 5–10%. Using a similar approach we find that the subgrid variability of the MOPITT CO column data ($22 \times 22 \text{ km}^2$ resolution) on the $2° \times 2.5°$ scale is typically about 5%. The actual representation error should be less since there are in general many MOPITT observations averaged over the $2° \times 2.5°$ model grid scale. In fact, in the absence of clouds, the MOPITT cross-track swath (612 km) is sufficient to provide full coverage of a grid square.

[35] The observational error displayed in Figure 4 for the MOPITT data is thus mainly contributed by the forward model error. This forward model error includes contributions from transport and chemistry, as well as an "aggregation error" describing the errors on the assumed spatial and temporal variations of sources for individual components of the state vector [Kaminski et al., 2001]. For purpose of the inverse analysis we must assume that the forward model error is unbiased. Bey et al. (submitted manuscript, 2004) examined the result of different GEOS-CHEM sampling offsets in the comparison to TRACE-P observations and showed that the transport error at least is largely unbiased.

3.3. Error Correlation

[36] Correlation of forward model errors must be resolved for dense aircraft or satellite observations. Previous chemical data assimilation studies of satellite observations, which employed a mathematical framework similar to our inverse model analysis, assumed a fixed correlation length scale [Lamarque et al., 1999; Khattatov et al., 2000; Clerbaux et al., 2001; Lamarque and Gille, 2003]. We use here the approach of Jones et al. [2003] to provide a more detailed characterization of the error correlation structure. This approach is based on the so-called "NMC method" [Parish and Derber, 1992]. It uses the error covariance between pairs of successive chemical forecasts of CO conducted during the TRACE-P mission with the same GEOS-3 meteorological product as used here and updated every 12 hours (Bey et al., submitted manuscript, 2004). By examining the differences in forecasts for the same end point but different time horizons (48 versus 24 hours), one obtains a representation of the forecast error, which is assumed to have the same structure as the model transport error [Jones et al., 2003]. One then scales this structure with the diagonal terms of $\mathbf{S}_\Sigma$ previously determined from the RRE analysis (section 3.1) to obtain the full structure of $\mathbf{S}_\Sigma$. Jones et al. [2003] found that the scaling factors when applying this method to the TRACE-P observations of CO were about a factor of two for forecasts separated by 24 hours. We find a similar result for the MOPITT data. The covariance structure of the model error is calculated from statistics for the ensemble of days of the TRACE-P mission and is assumed to be the same for all days.

[37] The error covariance structure from the NMC method is complicated to construct and requires the

availability of chemical forecasts by the forward model for the period of observations. It would be advantageous if we could parameterize the results in terms of a mean correlation length scale, as used in the previous studies cited above. To this end we fitted the NMC correlations $r(d)$ for the MOPITT CO column observations separated by a distance d as a second-order autoregressive function of the form:

$$r(d) = \left(1 + {}^{d}\!/_{L}\right) \exp\left({}^{-d}\!/_{L}\right) \quad (16)$$

where $L = 147$ km is a characteristic length scale (which corresponds to a 1/e drop-off at 320 km). The previous data assimilation studies cited above used an e-folding correlation length scale of 1000 km. We will examine the sensitivity of the inversion to the use of the simplified form of the error covariance structure represented by equation (16).

4. Selection of the State Vector

[38] We wish to select a suitable ensemble of source regions and source types as the state vector for the inverse model, given the set of observations (MOPITT or TRACE-P) used to constrain the solution. We start from a plausible ensemble of 16 elements including 12 geographical regions (Figure 3), plus additional separation of anthropogenic and biomass burning sources for 4 regions (SE Asia, Indonesia, S. China, and India) where daily resolution of biomass burning emissions [Heald et al., 2003a] might possibly provide a distinct signal. We construct the Jacobian for this 16-element state vector using the forward model, carry out the inversion to obtain $\hat{\mathbf{x}}$ and $\hat{\mathbf{S}}$ by equations (3) and (4), and then proceed to establish which elements are actually constrained by the MOPITT and TRACE-P observing systems.

[39] Previous inverse model studies [Palmer et al., 2003a; Kasibhatla et al., 2002] diagnosed which state vector elements could be constrained from the observing system by using averaging kernels for the inversion (**A**):

$$\mathbf{A} = \mathbf{I} - \hat{\mathbf{S}}\mathbf{S}_a^{-1} \quad (17)$$

However, this requires confidence in the characterization of $\hat{\mathbf{S}}$ by equation (4). As the number of observations becomes very large, $\hat{\mathbf{S}}$ becomes very small because of the assumption that the observational error is unbiased and Gaussian. The assumption is not strictly correct, and hence $\hat{\mathbf{S}}$ is artificially small; the averaging kernels then give an overly optimistic measure of the constraints on sources from the observing system.

[40] We use instead a two-step approach to select an appropriate state vector from the above 16 elements. First we examine the error correlation matrix whose elements (r_{ij}) are obtained by normalizing $\hat{\mathbf{S}}$ (elements $\hat{s}_{ij}$):

$$r_{ij} = \frac{\hat{s}_{ij}}{\sqrt{\hat{s}_{ii}}\sqrt{\hat{s}_{jj}}} \quad (18)$$

[41] The error correlation matrices for both the TRACE-P and MOPITT observations indicate that biomass burning and anthropogenic sources within a geographical region are actually highly correlated for all four regions where we

attempted to separate them. Therefore we merge these two source types in our reduced state vector and conduct only a geographical separation. In addition, we find that we cannot separate source signatures from Korea and Japan, and therefore we merge these two sources. The resulting state vector consists of 11 elements, listed in Table 1.

[42] To further assess the independence of the 11 elements in our state vector for the MOPITT observing system, we conducted a singular value decomposition of the error-normalized Jacobian matrix $\tilde{\mathbf{K}} = \mathbf{S}_{\Sigma}^{-1/2}\mathbf{K}\mathbf{S}_a^{1/2}$, defined by Rodgers [2000] as the "prewhitened" Jacobian for the system. The number of singular values greater than unity indicates the effective rank of $\tilde{\mathbf{K}}$, i.e., the number of pieces of information that can be extracted above the noise of the system [Rodgers, 2000]. For our 11 element state vector we find 10 significant singular vectors representing combinations of the state vector elements. Inspection of these singular vectors (Figure 5) indicates that sources in Japan and Korea cannot be constrained, even when grouped together. This is because of the large Chinese source upwind and the lack of sensitivity of MOPITT to the lower troposphere (as mentioned in section 2.2.2). Although the observation system is able to estimate European and the rest of the world sources, these results will not be discussed here given that our observations are limited to the Asian region. We do not aim to rigorously constrain non-Asian sources.

[43] The TRACE-P observations, which are limited to the Asian outflow region over the NW Pacific (Figure 1), do not contain as much information as MOPITT toward resolving CO sources in Asia. Inspection of the error correlation matrix for the solution to the 16-component state vector using the TRACE-P aircraft observations indicates strong correlations between India, Europe, and the rest of the world sources. Singular value decomposition of the corresponding $\tilde{\mathbf{K}}$ matrix reveals only 4 significant singular vectors (Figure 5). On the basis of the data in Figure 5 we choose a six-component state vector for the TRACE-P observing system consisting of (1) northern China, Japan and Korea; (2) central and western China; (3) southern China; (4) SE Asia; (5) the Philippines; and (6) the rest of the world. The state vector for the aircraft observations therefore forms a 6-element subset of the state vector for the MOPITT observations (section 6).

5. Constraints on CO Sources From MOPITT Observations

5.1. Best Case Estimate

[44] We now apply the inverse model analysis described in sections 2 and 3 to constrain Asian sources of CO from the MOPITT observations (constraints from the TRACE-P observations will be discussed in section 6). MOPITT observations of CO are made twice daily at 1030 LT and 2230 LT. We find that the a posteriori solutions to the inverse analysis differ significantly when only the morning or evening overpasses are employed in the inversion (Figure 6). This difference is more than a factor of 2 for some sources. It is likely due to differences in data quality or biases that are not adequately described. Validation of MOPITT with aircraft measurements of vertical profiles has been limited so far to daytime observations [Jacob et al., 2003; Emmons et al., 2004]. Owing to decreased thermal contrast, the retrieval of nighttime concentrations is more
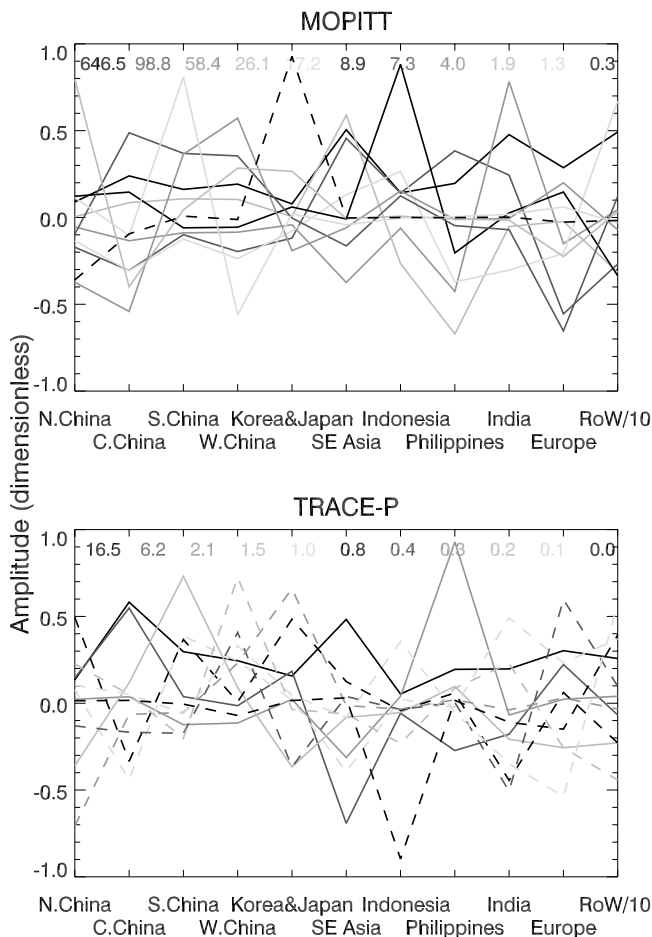
Figure 5. Singular vectors of the prewhitened Jacobian $\tilde{\mathbf{K}}$ matrix for the 11-element state vector given in Table 1 for (top) the MOPITT observations and (bottom) the aircraft observations. Each line represents one singular vector. As an example: the vector corresponding to the green solid line for the TRACE-P observations includes strong signatures for sources in the Philippines and SE Asia. The singular values corresponding to each vector are shown at the top of the figure. The singular vectors which cannot be retrieved above the noise in the system are indicated by the dotted lines. See color version of this figure at back of this issue.

challenging especially over land [*Deeter et al.*, 2003]. The decrease in thermal contrast also shifts the vertical sensitivity of the MOPITT instrument upward, reducing the ability to observe low altitudes where CO concentrations are highest. *Crawford et al.* [2004] found that nighttime observations of CO by MOPITT over the Pacific were less variable than daytime observations, which they attributed to an increase in the sensitivity of the retrieval to surface emissivity at night. We choose to use the daytime overpasses only in the results that follow. The morning solution shown in Figure 6 is referred to as our "best case."

[45] A posteriori source estimates for our best case are given in Table 1 and shown in red in Figure 7. The a posteriori errors as determined from $\hat{\mathbf{S}}$, are smaller than the widths of the symbols. Regions dominated by fossil fuel emissions such as China, Japan, and Korea are generally underestimated in the a priori inventory. Regions dominated

by biomass burning and biofuels, such as SE Asia and India, are greatly overestimated (by up to a factor of 2). Using our best case a posteriori sources for CO in the GEOS-CHEM simulation greatly improves the simulation of MOPITT and TRACE-P observations, as shown in Figures 8 and 9. The mean bias in the model compared to MOPITT is reduced from −4.4% to −0.6%. The mean bias compared to the TRACE-P observations, which are not employed to constrain this inverse solution and therefore provide an independent point of comparison, is also substantially reduced (from −14% to −5% on average in the boundary layer below 3 km).

5.2. Sensitivity Analysis

[46] The MAP inverse solution provides an estimate of the error covariance $\hat{\mathbf{S}}$ on the a posteriori sources (equation (4)). As shown in Figure 6 this error is small (less than 1 Tg for all sources). We pointed out previously that a very large number of observations, as is available from MOPITT, tends to result in a very small a posteriori error variance through the assumptions that errors are unbiased, Gaussian, representatively sampled, and not correlated from day to day. None of these assumptions are exactly correct, and therefore we expect $\hat{\mathbf{S}}$ to be too low.

[47] A better assessment of the error can be obtained by conducting an ensemble of inversions [*Peylin et al.*, 2002] addressing in different ways the error characterization, temporal averaging of observations [*Law et al.*, 2003], and aggregation errors [*Kaminski et al.*, 2001; *Kaminski and Heimann*, 2001; *Peylin et al.*, 2001]. We conducted such an ensemble of sensitivity inversions, listed in Table 2, and the corresponding range of solutions is shown as black bars in Figure 7. Although we consider them to be inferior in quality to our best case, they are all viable inversions and all produce very small a posteriori errors. As we see from Figure 7, the range of solutions from the different inversions is substantially larger than the a posteriori errors, which indicates that the solution is more sensitive to
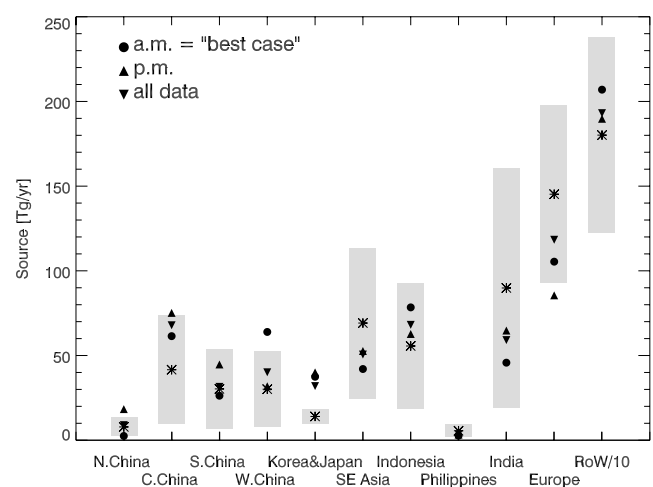
Figure 6. Sensitivity of the a posteriori CO source estimates to data selection for the MOPITT observations (corresponding to sensitivity tests 1, 2, and 3 in Table 2). Stars and shaded gray bars indicate a priori estimates and uncertainties. RoW refers to rest of world. A posteriori errors ($\hat{\mathbf{S}}$) are smaller than the width of the symbols.
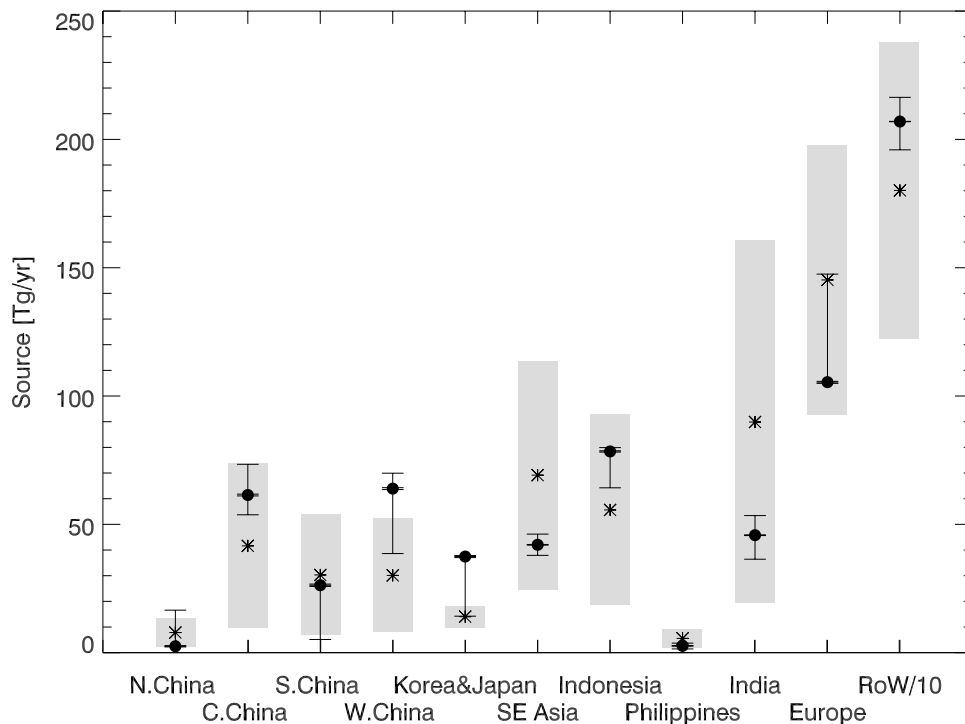
Figure 7. A posteriori CO source estimates constrained by the MOPITT morning observations. Stars and shaded gray bars indicate a priori estimates and uncertainties. The range of a posteriori solutions, corresponding to test cases 1, 4–12 (shown individually in Figures 10 and 11) discussed in the text, is shown by the black bar. The "best case" solution (shown in Table 1) is indicated by black circles. The a posteriori error associated with this solution is shown and is smaller than the width of the symbols.

modifications to the inverse system than the reported a posteriori errors would suggest. To obtain a true distribution of solutions, one would randomly perturb different aspects of the inversion simultaneously; therefore our range is likely a conservative estimate. In what follows we discuss more specifically this sensitivity.

5.2.1. Sensitivity to Observational Error

[48] The sensitivity of the a posteriori results to the characterization of errors is shown in Figure 10 in comparison with our best case inversion. The solution is relatively insensitive to the specification of the a priori error covariance (S_a), as expected since the number of observations is so large as to dwarf the contribution from the a priori in the cost function (equation (2)). Ignoring the spatial error correlation in the observations (blue triangles) leads to source estimates that differ by 10–50% relative to the best case. The solution obtained when the correlations are parameterized as a single correlation length scale of 147 km (see section 3.3) can differ from the solution obtained with the full correlation fields by a similar factor, implying that the detailed error correlation structure is important to resolve. Setting the observational error variance uniformly at 7% (the mean of S_Σ within the geographical domain of the observations) or 20% results in significant differences (up to 40%) in the solution for some sources, as the information conveyed by the geographically varying errors has been lost. We also tested the sensitivity of the solution to a potential underestimate in error by adding a uniform 10% error to S_Σ. We find that this has little impact on the solution.

5.2.2. Sensitivity to Temporal Resolution

[49] Previous inverse modeling studies of CO have employed monthly mean observations from MOPITT [*Arellano et al.*, 2004] or from NOAA/CMDL surface sites [*Bergamaschi et al.*, 2000; *Pétron et al.*, 2002; *Kasibhatla et al.*, 2002]. Daily observations, by resolving synoptic structures, should provide greater information. However, the model transport error when applied to daily data is also likely greater. We performed the inversion for Asian sources with MOPITT observations sampled at three temporal resolutions: (1) the native daily data, (2) weekly averages, and (3) a 7-week average corresponding to the duration of the TRACE-P mission. Figure 11 compares the results. For (2) and (3) we reduced the observational error by the square root of the number of days incorporated in the averaged data; this assumes (using the central limit theorem) that each day represents an independent random realization of the observational error. We also assume in this comparison that errors are uncorrelated, as it is unclear how the error correlation structure would evolve with temporal resolution. For 9 of the 11 elements of the state vector, the a posteriori solutions obtained using weekly averages are in better agreement with those using the daily data than those using the mission mean data. The only exceptions are Europe and the rest of the world. For the majority of the sources, the a posteriori solution obtained with daily observations is further from the a priori estimate than either of the estimates obtained using mean fields. Singular vector decomposition of the $\bar{K}$ matrices (section 4) shows that the number of independent pieces of information that can be resolved by the inversion
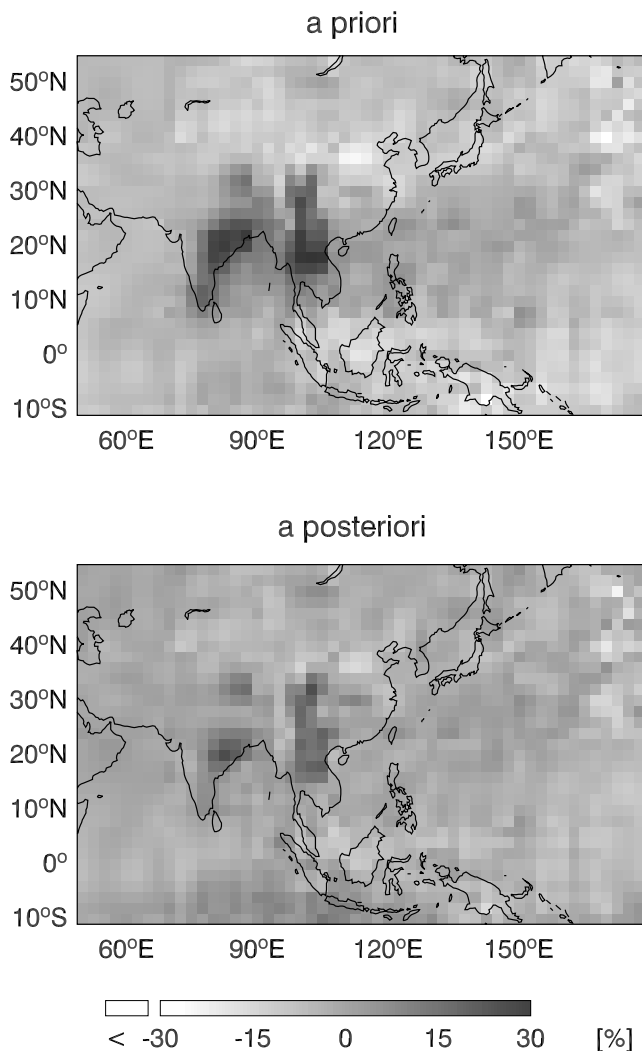
a priori

a posteriori

Figure 8. GEOS-CHEM model bias in the simulation of MOPITT observations when either the a priori or the best case a posteriori CO sources (Table 1) are used as input to the model. Bias is defined as the mean of the difference between simulated and observed concentrations averaged over the spring 2001 observing period. Color scale is saturated at 30% but model bias in the a priori comparison ranges up to 75% over SE Asia. See color version of this figure at back of this issue.

decreases from 10 with the daily observations to 9 with weekly averages and 7 with the 7-week average. Differences in the solution may therefore reflect the reduction in information content when the temporal resolution of the observations is degraded. However, the solution using the daily data is also more influenced by plume events, for which the observational error may be particularly large [*Kiley et al.*, 2003] and not adequately described by the RRE method [*Palmer et al.*, 2003a].

5.2.3. Sensitivity to Aggregation Error

[50] Aggregation errors are the result of incorrect spatial or temporal distribution of emissions within a region described as a single element of the state vector. Their impact was first examined by *Kaminski and Heimann* [2001] and *Kaminski et al.* [2001] for CO_2 inversions, who recommended that they be avoided by resolving surface fluxes from each model grid square in the state vector. However, *Peylin et al.* [2001] pointed out that such an approach ignores the a priori knowledge of spatial coherence of emissions. This coherence could conceivably be accounted for in the specification of the a priori errors, but the resulting matrices would be unmanageably large.

[51] In an effort to examine what impact the aggregation error may have on the results presented here, we conducted sensitivity studies with state vectors representing different degrees of aggregation for Asian sources. These are the 16- and 11-element state vectors described previously, a 9-element vector (where India and Europe are aggregated with the rest of the world), and a 6-element vector (see *x* axis of Figure 12). Results from each inversion were then summed over the 6 elements of the coarsest resolution inversion and compared (Figure 12). Solutions obtained with the 9- and 6-element state vector are similar, however substantial differences are found when comparing with the larger 11- or 16-element state vector solution. Differences extend beyond
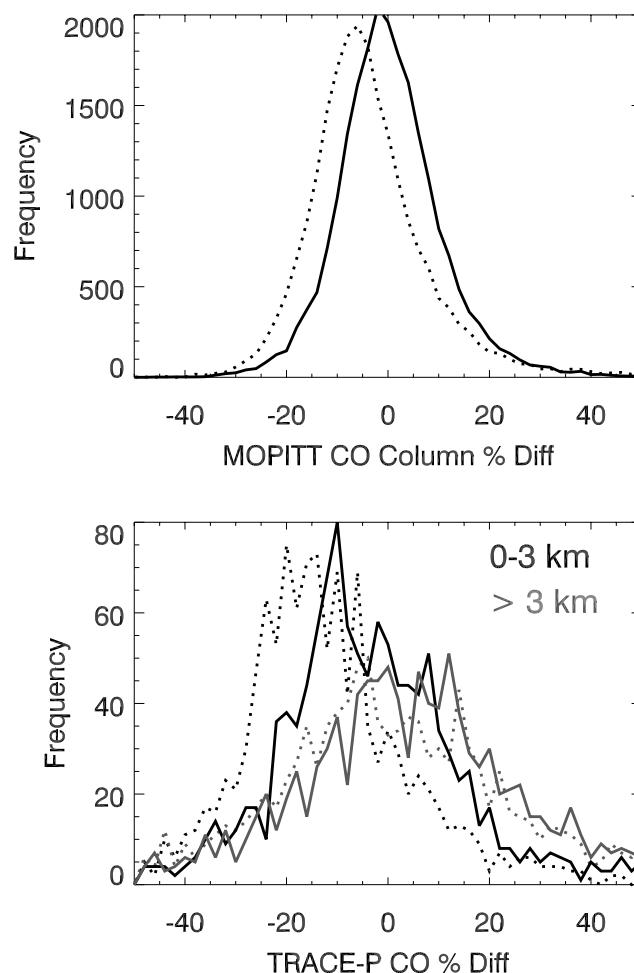
Figure 9. GEOS-CHEM model bias in the simulation of (top) MOPITT observations or (bottom) TRACE-P observations when either the a priori (dotted) or the best case a posteriori (thick) CO sources (Table 1) are used as input to the model. Bias is defined as the mean of the difference between simulated and observed concentrations averaged over the spring 2001 observing period. See color version of this figure at back of this issue.
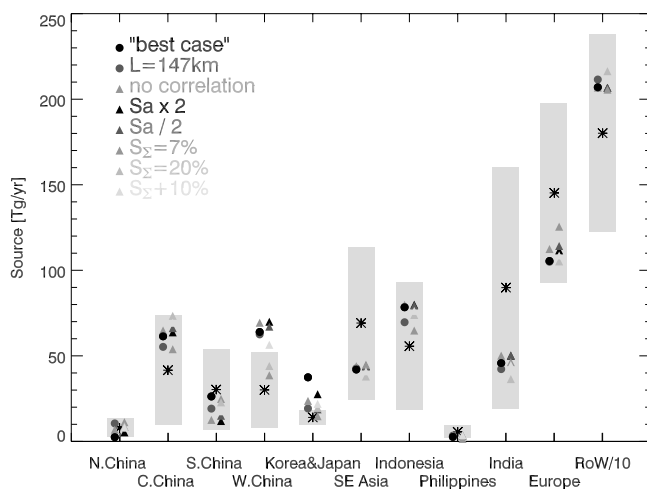
Table 2. Inversion Sensitivity Tests

Test Case[a]	State Vector Size	Data Selection	Temporal Resolution	Error Characterization
1 = best case	11	MOPITT (morning)	daily	standard, NMC correlation
2	11	MOPITT (evening)	daily	standard, NMC correlation
3	11	MOPITT (morning and evening)	daily	standard, NMC correlation
4	11	MOPITT (morning)	daily	standard, L = 147km correlation
5	11	MOPITT (morning)	daily	standard, uncorrelated
6	11	MOPITT (morning)	daily	Sa/2, uncorrelated
7	11	MOPITT (morning)	daily	Sa * 2, uncorrelated
8	11	MOPITT (morning)	daily	S_Σ = 7%, uncorrelated
9	11	MOPITT (morning)	daily	S_Σ = 20%, uncorrelated
10	11	MOPITT (morning)	daily	S_Σ + 10%, uncorrelated
11	11	MOPITT (morning)	weekly	S_Σ for wk, uncorrelated
12	11	MOPITT (morning)	mean (7 weeks)	S_Σ for mean, uncorrelated
13	16	aircraft	n/a	standard, uncorrelated
14	16	MOPITT (morning)	daily	standard, uncorrelated
15	16	MOPITT (morning)	daily	standard, NMC correlation
16	9	aircraft	n/a	standard, NMC correlation
17	9	MOPITT (morning)	daily	standard, NMC correlation
18	6	aircraft	n/a	standard, NMC correlation
19	6	MOPITT (morning)	daily	standard, NMC correlation
20	6	MOPITT (morning)	daily	remove 6% bias, NMC correlation
21	6	MOPITT (morning) (10−45°N, 120−150°E)	daily	standard, NMC correlation

[a]The range of solutions in Figure 7 is defined by the results from test cases 1, 4−12, 14, 17, and 19.

the a priori uncertainty for the (1) central/western China and (2) northern China/Japan/Korea sources, suggesting that aggregation error can affect these solutions. In addition, the differences in SE Asian estimates indicate that aggregation errors in adjoining regions may impact the solution in regions that are not aggregated. These differences emphasize the importance of carefully selecting the state vector.
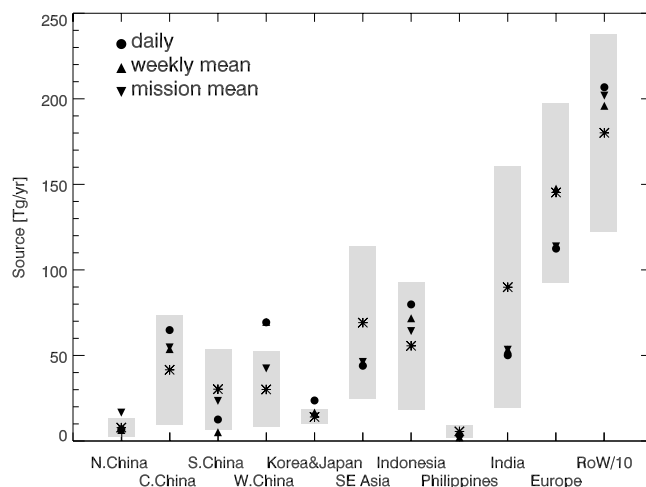
6. Comparing Aircraft and Satellite

[52] The analysis of section 4 indicates that the TRACE-P aircraft observations can be used to constrain only a subset of the regional Asian sources constrained by the MOPITT observations. The consistency of the constraints between these two very different data sets is examined here. Comparison of the a posteriori solutions obtained using the 6-element state vector constrainable by TRACE-P aircraft observations (see section 4) is shown in Figure 13. The satellite and aircraft observations provide qualitatively similar constraints on Asian CO sources but there are some quantitative differences. The most pronounced differences are for the SE Asia and the rest of the world sources. Although both aircraft and satellite observations indicate that a priori emissions in SE Asia are too high, the satellite
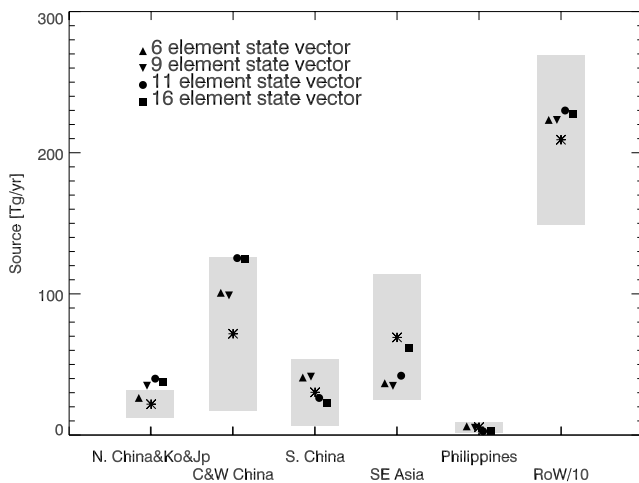

Figure 10. Sensitivity of the a posteriori CO source estimates to the error characterization for the MOPITT observation system. Results from a number of sensitivity test cases with modified error assumptions (cases 4−10 of Table 2) are shown together with the best case. Stars and shaded gray bars indicate a priori estimates and uncertainties. See color version of this figure at back of this issue.

Figure 11. Sensitivity of the a posteriori CO source estimates to the temporal resolution of the MOPITT observations (corresponding to cases 5, 11, and 12 in Table 2). Stars and shaded gray bars indicate a priori estimates and uncertainties.

Figure 12. Sensitivity of the a posteriori CO source estimates to aggregation error for the MOPITT observations (corresponding to cases 1, 15, 17, and 19 in Table 2). Stars and shaded gray bars indicate a priori estimates and uncertainties.

observations imply a factor of 2 overestimate while the aircraft observations indicate a much larger factor. The SE Asian influence in the TRACE-P data over the NW Pacific is mainly in the middle and upper troposphere [*Liu et al.*, 2003], where model transport errors could be relatively large. *Allen et al.* [2004] previously showed that the TRACE-P CO data provide only a loose constraint on biomass burning CO emissions. The MOPITT data, which include observations over the continent and over the Indian Ocean, are likely better able to quantify the emissions. MOPITT validation profiles conducted during the TRACE-P mission indicated a 6% mean positive bias in the MOPITT column observations [*Jacob et al.*, 2003]. The impact on the solution when this 6% bias is removed from the MOPITT observations is minimal but does tend to marginally improve the agreement with the TRACE-P inversion (Figure 13).

[53] The better capability of MOPITT versus TRACE-P for constraining Asian sources could reflect in MOPITT either the increased data density in Asian outflow over the Pacific, or the addition of observations over the continent and over the Indian Ocean, which receives boundary layer outflow from the Indian subcontinent and SE Asia during the spring [*Lelieveld et al.*, 2001]. To distinguish these two effects we considered a subset of the MOPITT observations limited to the outflow region sampled by the aircraft (10−45°N, 120−150°E) and calculated the corresponding singular values of $\mathbf{K}$. We found only 5 significant singular values, similar to the aircraft observations. Thus geographical extent is key. The inversion using this restricted MOPITT observation domain yields solutions for the SE Asia source as well as the other Asian sources (except S. China) that are more consistent with those constrained by the aircraft. We further find that by adding MOPITT observations over the Indian Ocean (10°S−10°N, 50−95°E) to the observations over the TRACE-P outflow region we increase the number of significant singular vectors to 8. We conclude

that the ability to constrain sources from atmospheric observations is substantially enhanced by being able to make observations over all outflow pathways as well as the source regions.

7. Implications for Asian CO Sources

[54] We now discuss our inverse model results for Asian CO sources in the context of the a priori bottom-up estimates and previous literature. Our total for east and south Asian sources is 361 Tg yr^{-1}, compared to the a priori estimate of 344 Tg yr^{-1}. China, Korea, and Japan make up 53% of that total (192 Tg yr^{-1}). The a priori anthropogenic emissions of *Streets et al.* [2003] appear to be too low, particularly in China. Previous TRACE-P studies have suggested that this is due to under-reporting of domestic coal burning [*Carmichael et al.*, 2003; *Streets et al.*, 2003] and inefficient industrial sources and power plants [*Suntharalingam et al.*, 2004]. More recent work by D. G. Streets indicates that the primary cause is underestimation of the CO emission rates of small industrial coal facilities (D. G. Streets et al., manuscript in preparation, 2004). *Streets et al.* [2003] also discuss the large uncertainty associated with the biofuel source in India, which makes up over 40% of the a priori emissions for that region. The inversion diagnoses a factor of 2 overestimate for the Indian source.

[55] The Asian source estimates derived in this work are compared in Table 3 with other inverse model studies reported in the literature. Our values are expressed as annual means, even though the observational constraints are only for spring, by assuming effectively that the relative seasonal cycle of the sources is known. Comparison of inverse model estimates is often problematic as studies focus on different years and define the state vector differently.

[56] Our inversion using TRACE-P aircraft observations agrees well, as expected, with results obtained by *Palmer et*
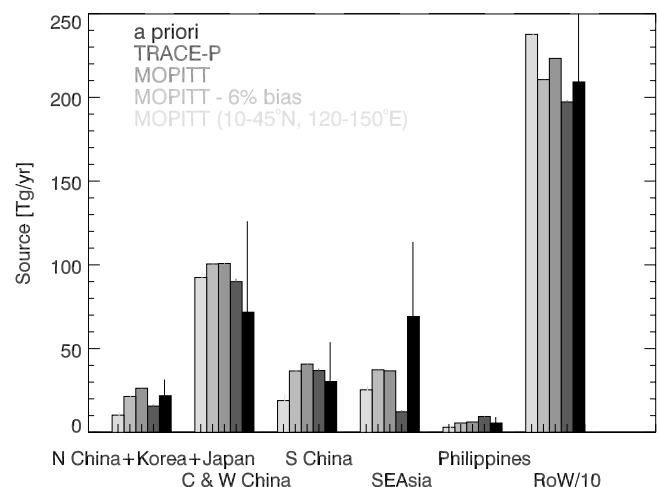
Figure 13. Comparison of a posteriori source estimates for CO as constrained by the aircraft and MOPITT observations using a state vector containing only the six regions identified in the figure (test cases 18–21). Included are results for MOPITT corrected by its 6% positive column bias, and for MOPITT sampled over the TRACE-P flight region only (10−45°N, 120−150°E). See color version of this figure at back of this issue.

Table 3. Inverse Model Estimates of Annual Asian Sources of CO (Tg yr^{-1})[a]

Reference	Observations (Year)	Forward Model	Bottom-up Constraints[b]	Regions	A Priori	A Posteriori
This work[c]	MOPITT satellite [TRACE-P aircraft] (2001)	GEOS-CHEM	FF/BF: *Streets et al.* [2003] BB: *Heald et al.* [2003a]	China, Korea, and Japan	124	192 (142)[d]
				SE Asia and Philippines	75	45 [22]
				India	90	46
				Indonesia	56	78
Palmer et al. [2003a, 2003b]	TRACE-P aircraft (2001)	GEOS-CHEM	FF/BF: *Streets et al.* [2003] BB: *Heald et al.* [2003a]	China FF/BF	109	168
				China BB	19	12
				Korea and Japan	19	26
				SE Asia, Philippines, and Indonesia	125	33
Carmichael et al. [2003]	TRACE-P aircraft (2001)	CFORS/STEM-2K1	FF/BF: *Streets et al.* [2003] BB: *Woo et al.* [2003]	Asia[e] FF/BF	211	380[f]
				Asia BB	67	67[g]
Allen et al. [2004]	TRACE-P aircraft (2001)	UMD CTM	FF/BF: *Streets et al.* [2003] *Woo et al.* [2003] BB: *Woo et al.* [2003]	Asia[h] FF/BF	189	301 ± 67
				Asia BB	57[i]	27 ± 26[j]
Arellano et al. [2004]	MOPITT satellite (2000)	GEOS-CHEM	FF/BF: EDGAR v2 [*Olivier et al.*, 1996] BB: *van der Werf et al.* [2003]	China, Korea, and Japan (FF/BF)	109	204
				SE Asia, Philippines, and Indonesia (FF/BF)	41	75
				India and Middle East (FF/BF)	88	144
				SE Asia, Philippines, Indonesia, and India (BB)	42	96
Pétron et al. [2002]	CMDL surface (1990−1996[k])	MOZART	FF/BF: EDGAR v2 [*Olivier et al.*, 1996] BB: *Granier et al.* [2000]	Asia[l] FF/BF	78	120−124
				Asia BB	317	566−584
Kasibhatla et al. [2002]	CMDL surface (1994[m])	GEOS-CHEM	FF/BF: EDGAR v2 [*Olivier et al.*, 1996] BB: EDGAR	Asia[n] FF/BF	240	350−380
				Asia BB	59	112−123

[a]All of these studies employ Bayesian synthesis inversions, except for *Carmichael et al.* [2003] and *Allen et al.* [2004] who did forward comparisons of the TRACE-P observations with a regional or global model simulations respectively.

[b]A priori information for fossil fuel (FF), biofuel (BF), and biomass burning (BB) sources. The sources include both direct emission and chemical production from coemitted nonmethane volatile organic compounds (NMVOCs).

[c]See Table 1 for further detail on the geographical distribution of sources.

[d]Square brackets denote results obtained with TRACE-P aircraft observations.

[e]Asia defined as China, Japan, Korea, SE Asia, Philippines, Indonesia, and India.

[f]Obtained by doubling the domestic sector contribution to improve agreement with TRACE-P observations.

[g]The biomass burning source was not modified in this study.

[h]Asia defined as $60°-158°$E, $13°$S$-54°$N.

[i]March 2001 estimates have been scaled to annual totals using the seasonal cycle of *Duncan et al.* [2003].

[j]Assuming the relative climatological seasonal variation of *Duncan et al.* [2003] to scale the March estimate of 8.5 ± 8.3 Tg from *Allen et al.* [2004] to a full year.

[k]Observations only. Meteorological fields from 1985−1989 and emissions for 1990.

[l]Asia includes Siberia.

[m]Observations and meteorological fields. Emissions from early 1990s.

[n]Including China, Japan, Korea, SE Asia , the Philippines, Indonesia, India, and the Middle East.

al. [2003a] for 2001. There are some differences due to error characterization as well as state vector definition. Both studies show that (1) emissions from China, Korea, and Japan are underestimated in the *Streets et al.* [2003] inventory (by 40% in *Palmer et al.* [2003a], compared to 15% here when using the aircraft observations or 55% when using the MOPITT observations), and (2) emissions from SE Asia in the work of *Heald et al.* [2003a] are drastically overestimated. *Palmer et al.* [2003a] suggest that SE Asian emissions should be decreased by 74%, whereas this work decreases this source by 71% when using TRACE-P observations or 40% when using MOPITT observations.

[57] *Carmichael et al.* [2003] simulated the TRACE-P observations of CO with a regional CTM and concluded that domestic emissions from central China are underesti-

mated in the *Streets et al.* [2003] inventory by a factor of 3−5. They doubled the domestic sector in Asia (including India) to arrive at a total anthropogenic (fossil fuel and biofuel) estimate of 380 Tg yr^{-1} which is larger than our total Asian source (including biomass burning) of 361 Tg yr^{-1}. This suggests that the factor of 2 increase cannot be extended to all of Asia.

[58] A similar study by *Allen et al.* [2004] linearly fit the bulk of the TRACE-P observations to a CTM simulation in order to obtain scaling factors for Asian anthropogenic and biomass burning sources. They did not separate sources geographically. Scaling factors for the *Streets et al.* [2003] anthropogenic sources were 1.59 ± 0.34, implying a best estimate of 301 ± 67 Tg. Scaling factors for the *Woo et al.* [2003] biomass burning sources were 0.47 ± 0.46, implying

a best estimate of 8.5 ± 8.3 Tg for Asia in March. Assuming the *Duncan et al.* [2003] seasonal variation this corresponds to an annual Asian biomass burning source of 27 ± 26 Tg, which is substantially smaller than our estimate as well as results from previous studies (see Table 3).

[59] *Arellano et al.* [2004] used monthly mean MOPITT observations for 2000 to infer that anthropogenic sources in China, Japan and Korea in the EDGARV2/GEIA inventory [*Olivier et al.*, 1996] are underestimated. They obtained an a posteriori source of 204 Tg yr^{-1}, which is close to our estimate (192 Tg yr^{-1}). Their anthropogenic estimate for SE Asia, India and Indonesia (219 Tg yr^{-1}) is substantially larger than our estimate of the total (anthropogenic + biomass burning) source for that region (169 Tg yr^{-1}), given that the large biomass burning source is not included in their value.

[60] The total Asian sources obtained by *Pétron et al.* [2002] (686–708 Tg yr^{-1}) and *Kasibhatla et al.* [2002] (462–503 Tg yr^{-1}) using CMDL observations are much larger than the totals we obtain here (361 Tg yr^{-1} when including India and Indonesia). Although these inversions were done for different years, it is unlikely that interannual variability in emissions can explain the difference. Biomass burning emissions in SE Asia for 1979–2001 appear to vary interannually by at most 50% according to the TOMS aerosol index (AI) record [*Heald et al.*, 2003a] (note that this does not include India or Indonesia). CMDL sites have been positioned to capture background conditions, and are less suited to constrain Asian sources than the MOPITT or TRACE-P observations. Inverse analysis of CMDL observations to constrain Asian sources relies strongly on the data from a few Pacific island sites that are far removed from these sources and hence may be particularly susceptible to model biases in transport.

8. Conclusions

[61] We used an inverse model analysis to compare the top-down constraints on Asian sources of CO in spring 2001 from (1) daily MOPITT satellite observations of CO columns over Asia and the neighboring oceans, and (2) aircraft observations of CO mixing ratios in Asian outflow from the TRACE-P aircraft mission over the NW Pacific. The inversion applied the maximum a posteriori Bayesian synthesis method with the GEOS-CHEM chemical transport model as the forward model. Our objective was to determine if the satellite and aircraft provide consistent constraints on Asian CO sources, and whether these constraints are complementary or redundant.

[62] Proper characterization of the observational error and its covariant structure is critical for this analysis. We used the RRE method [*Palmer et al.*, 2003a] to quantify the observational error variance and its geographical pattern. Observational errors are typically 5–30% for both the satellite columns and aircraft mixing ratios, and are mainly contributed by the forward model error; instrument and representation errors are relatively small. The errors are highest over convective source regions. We estimated the spatial covariance of the transport error by applying the NMC method [*Parish and Derber*, 1992] to paired statistics of successive chemical forecasts. This provides a region-specific, nonisotropic description of error correlation between neighboring

measurements. The resulting horizontal length scale for the error correlation is typically about 150 km.

[63] We found that the MOPITT satellite and TRACE-P aircraft observations provide remarkably consistent constraints on Asian sources of CO, with the exception of SE Asia where MOPITT implies higher emissions. It appears that TRACE-P does not constrain SE Asian sources adequately due to the large transport errors involved in the lifting and subsequent advection of biomass burning effluents to the NW Pacific. The MOPITT observations provide ten independent pieces of information to constrain the geographical distribution of CO sources, as inferred from the effective rank of the prewhitened Jacobian. The TRACE-P observations provide only four, which do not appear to be independent from MOPITT and thus do not convey any complementary information. The greater information content from MOPITT is due to its ability to observe the Asian continent and outflow over the Indian Ocean, whereas the TRACE-P aircraft was not allowed to fly over the continent and could only sample the continental outflow over the Pacific. When MOPITT observations are sampled only over the TRACE-P flight domain we find that the number of independent pieces of information on CO sources drops to five, similar to the number for the TRACE-P aircraft observations. We conclude that future aircraft missions aimed at constraining continental emissions should fly if possible directly over the source region. An advantage of aircraft over satellites for constraining sources is the ability to measure a large number of species and exploit species-species correlations as source signatures. Several studies did this in TRACE-P by correlating CO with observations of halocarbons [*Palmer et al.*, 2003b], nitriles [*Li et al.*, 2003; *Singh et al.*, 2003], CO_2 [*Suntharalingam et al.*, 2004] and methane [*Xiao et al.*, 2004].

[64] We examined the consequences in the MOPITT inverse model analysis of deliberately degrading the temporal resolution of the observations or the geographical resolution of sources (i.e., dimension of the state vector). We found that selecting for daytime orbits (1030 LT) versus nighttime (2230 LT) yielded significantly different inversion results. We discarded the nighttime data because they are less sensitive to the lower troposphere and because they have so far not been validated (in contrast to the daytime data). This highlights the importance of satellite instrument validation so that data can be used accurately and effectively both in outflow and background conditions, for daytime and nighttime overpasses if applicable, and with as great a global extent as possible.

[65] Averaging the native daily MOPITT observations over a weekly timescale or over the 7-week duration of the TRACE-P mission led to significant loss of information in the inversion. This indicates that the native daily MOPITT data provide important information on sources that is lost in the temporal averaging. Aggregating Asian source regions (e.g., central and western China) in the state vector aliases the inverse model results for the merged source (aggregation error). This emphasizes the importance of conducting an eigenanalysis of the inverse modeling system to guide the selection of the state vector of sources.

[66] Inverse modeling by Bayesian synthesis yields artificially small errors on the a posteriori sources when one uses a very large number of observations, as from a satellite

instrument. As the number of observations tends toward infinity, the error on the a posteriori sources tends toward zero. This is because the observational error is assumed to be random, Gaussian, representatively sampled by the observations, and adequately characterized as to its covariance. None of these assumptions is strictly correct, and the consequences become increasingly important as the number of observations increases. As previously pointed out by *Peylin et al.* [2002] for CO_2 inversions, one cannot rely on a Bayesian synthesis inversion to provide a proper estimate of a posteriori errors. Ensemble modeling is necessary. This was done here by conducting a series of inverse model calculations with different reasonable assumptions regarding observational errors and temporal averaging, and using the results to define an envelope of solutions.

[67] We compared our a posteriori estimates of Asian CO sources to previous inverse model studies that used surface observations of CO concentrations from NOAA/CMDL sites or global monthly mean MOPITT observations. Estimates based on the MOPITT or TRACE-P data are lower than those based on the NOAA/CMDL data, possibly because of the paucity of the latter and the resulting greater sensitivity to CTM bias. All inverse model studies agree that current bottom-up emission inventories constrained with available socioeconomic and emission factor data underestimate anthropogenic sources in China. The most likely reason is under-reporting of industrial coal facilities. As our observational capability for mapping of atmospheric composition from space increases dramatically over the next decade, constraints from inverse model analyses should become increasingly useful for guiding the improvement of bottom-up emission inventories and enhance our ability to project future emissions.

References

Allen, D., K. Pickering, and M. Fox-Rabinovitz (2004), Evaluation of pollutant outflow and CO sources during TRACE-P using model-calculated, aircraft-based, and Measurements of Pollution in the Troposphere (MOPITT)-derived CO concentrations, *J. Geophys. Res.*, *109*, D15S03, doi:10.1029/2003JD004250.

Arellano, A. F., Jr., P. S. Kasibhatla, L. Giglio, G. R. van der Werf, and J. T. Randerson (2004), Top-down estimates of global CO sources using MOPITT measurements, *Geophys. Res. Lett.*, *31*, L01104, doi:10.1029/2003GL018609.

Bergamaschi, P., R. Hein, M. Heimann, and P. J. Crutzen (2000), Inverse modeling of the global CO cycle: 1. Inversion of CO mixing ratios, *J. Geophys. Res.*, *105*(D2), 1909–1927.

Berntsen, T., I. S. A. Isaksen, W. C. Wang, and X. Z. Liang (1996), Impacts of increased anthropogenic emissions in Asia on tropospheric ozone and climate—A global 3-D model study, *Tellus Ser. B*, *48*(1), 13–32.

Carmichael, G. R., et al. (2003), Evaluating regional emission estimates using the TRACE-P observations, *J. Geophys. Res.*, *108*(D21), 8810, doi:10.1029/2002JD003116.

Clerbaux, C., J. Hadji-Lazaro, D. Hauglustaine, and G. Megie (2001), Assimilation of carbon monoxide measured from satellite in a three-dimensional chemistry-transport model, *J. Geophys. Res.*, *106*(D14), 15,385–15,394.

Crawford, J. H., et al. (2004), Relationship between Measurements of Pollution in the Troposphere (MOPITT) and in situ observations of CO based on a large-scale feature sampled during TRACE-P, *J. Geophys. Res.*, *109*, D15S04, doi:10.1029/2003JD004308.

Deeter, M. N., et al. (2003), Operational carbon monoxide retrieval algorithm and selected results for the MOPITT instrument, *J. Geophys. Res.*, *108*(D14), 4399, doi:10.1029/2002JD003186.

Drummond, J. R., and G. S. Mand (1996), The Measurements of Pollution in the Troposphere (MOPITT) instrument: Overall performance and calibration requirements, *J. Atmos. Oceanic Technol.*, *13*, 314–320.

Duncan, B. N., R. V. Martin, A. C. Staudt, R. Yevich, and J. A. Logan (2003), Interannual and seasonal variability of biomass burning emissions constrained by satellite observations, *J. Geophys. Res.*, *108*(D2), 4100, doi:10.1029/2002JD002378.

Edwards, D. P., C. Halvorson, and J. C. Gille (1999), Radiative transfer modeling of the EOS Terra Satellite Measurements of Pollution in the Troposphere (MOPITT) instrument, *J. Geophys. Res.*, *104*, 16,755–16,775.

Emmons, L. K., et al. (2004), Validation of Measurements of Pollution in the Troposphere (MOPITT) CO retrievals with aircraft in situ profiles, *J. Geophys. Res.*, *109*, D03309, doi:10.1029/2003JD004101.

Fiore, A., D. J. Jacob, H. Liu, R. M. Yantosca, T. D. Fairlie, and Q. Li (2003), Variability in surface ozone background over the United States: Implications for air quality policy, *J. Geophys. Res.*, *108*(D24), 4787, doi:10.1029/2003JD003855.

Fuelberg, H. E., C. M. Kiley, J. R. Hannan, D. J. Westberg, M. A. Avery, and R. E. Newell (2003), Meteorological conditions and transport pathways during the Transport and Chemical Evolution over the Pacific (TRACE-P) experiment, *J. Geophys. Res.*, *108*(D20), 8782, doi:10.1029/2002JD003092.

Granier, C., J.-F. Muller, and G. Brasseur (2000), The impact of biomass burning on the global budget of ozone and ozone precursor, in *Biomass Burning and Its Inter-Relationships With the Climate System*, edited by J. L. Innes, M. Beniston, and M. M. Verstracke, pp. 69–85, Kluwer Acad., Norwell, Mass.

Hannan, J. R., H. E. Fuelberg, J. H. Crawford, G. W. Sachse, and D. R. Blake (2003), Role of wave cyclones in transporting boundary layer air to the free troposphere during the spring 2001 NASA/TRACE-P experiment, *J. Geophys. Res.*, *108*(D20), 8785, doi:10.1029/2002JD003105.

Heald, C. L., D. J. Jacob, P. I. Palmer, M. J. Evans, G. W. Sachse, H. B. Singh, and D. R. Blake (2003a), Biomass burning emission inventory with daily resolution: Application to aircraft observations of Asian outflow, *J. Geophys. Res.*, *108*(D21), 8811, doi:10.1029/2002JD003082.

Heald, C. L., et al. (2003b), Asian outflow and trans-Pacific transport of carbon monoxide and ozone pollution: An integrated satellite, aircraft, and model perspective, *J. Geophys. Res.*, *108*(D24), 4804, doi:10.1029/2003JD003507.

Intergovernmental Panel on Climate Change (IPCC) (2001), *Climate Change 2001: The Scientific Basis, Contribution of Working Group I to the Third Assessment Report of the Intergovernmental Panel on Climate Change*, edited by J. T. Houghton et al., Cambridge Univ. Press, New York.

Jacob, D. J., J. H. Crawford, M. M. Kleb, V. S. Connors, R. J. Bendura, J. L. Raper, G. W. Sachse, J. C. Gille, L. Emmons, and C. L. Heald (2003), Transport and Chemical Evolution over the Pacific (TRACE-P) aircraft mission: Design, execution, and first results, *J. Geophys. Res.*, *108*(D20), 9000, doi:10.1029/2002JD003276.

Jaeglé, L., D. A. Jaffe, H. U. Price, P. Weiss-Penzias, P. I. Palmer, M. J. Evans, D. J. Jacob, and I. Bey (2003), Sources and budgets for CO and O_3 in the northeastern Pacific during the spring of 2001: Results from the PHOBEA-II Experiment, *J. Geophys. Res.*, *108*(D20), 8802, doi:10.1029/2002JD003121.

Jones, D. B. A., K. W. Bowman, P. I. Palmer, J. R. Worden, D. J. Jacob, R. N. Hoffman, I. Bey, and R. M. Yantosca (2003), Potential of observations from the Tropospheric Emission Spectrometer to constrain continental sources of carbon monoxide, *J. Geophys. Res.*, *108*(D24), 4789, doi:10.1029/2003JD003702.

Kaminski, T., and M. Heimann (2001), Technical comment: Inverse modeling of atmospheric carbon dioxide fluxes, *Science*, *294*, 259.

Kaminski, T., P. J. Rayner, M. Heimann, and I. G. Enting (2001), On aggregation errors in atmospheric transport inversions, *J. Geophys. Res.*, *106*(D5), 4703–4715.

Kasibhatla, P., A. Arellano, J. A. Logan, P. I. Palmer, and P. Novelli (2002), Top-down estimate of a large source of atmospheric carbon monoxide associated with fuel combustion in Asia, *Geophys. Res. Lett.*, *29*(19), 1900, doi:10.1029/2002GL015581.

Khattatov, B. V., et al. (2000), Assimilation of satellite observations of long-lived chemical species in global chemistry transport models, *J. Geophys. Res.*, *105*(D23), 29,135–29,144.

Kiley, C. M., et al. (2003), An intercomparison and evaluation of aircraft-derived and simulated CO from seven chemical transport models during the TRACE-P experiment, *J. Geophys. Res.*, *108*(D21), 8819, doi:10.1029/2002JD003089.

Krol, M., P. J. van Leeuwen, and J. Lelieveld (1998), Global OH trend inferred from methylchloroform measurements, *J. Geophys. Res.*, *103*(D9), 10,697–10,711.

Lamarque, J.-F., and J. C. Gille (2003), Improving the modeling of error variance evolution in the assimilation of chemical species: Application to MOPITT data, *Geophys. Res. Lett.*, *30*(9), 1470, doi:10.1029/2003GL016994.

Lamarque, J.-F., B. V. Khattatov, J. C. Gille, and G. P. Brasseur (1999), Assimilation of Measurement of Air Pollution from Space (MAPS) CO in a global three-dimensional model, *J. Geophys. Res.*, *104*(D21), 26,209–26,218.

Law, R. M., P. J. Rayner, L. P. Steele, and I. G. Enting (2003), Data and modelling requirement for CO2 inversions using high-frequency data, *Tellus, Ser. B*, *55*, 512–521.

Lelieveld, J., et al. (2001), The Indian Ocean Experiment: Widespread air pollution from south and southeast Asia, *Science*, *291*, 1031–1036.

Li, Q., D. J. Jacob, R. M. Yantosca, C. L. Heald, H. B. Singh, M. Koike, Y. Zhao, G. W. Sachse, and D. G. Streets (2003), A global three-dimensional model analysis of the atmospheric budgets of HCN and CH_3CN: Constraints from aircraft and ground measurements, *J. Geophys. Res.*, *108*(D21), 8827, doi:10.1029/2002JD003075.

Liu, H., D. J. Jacob, I. Bey, R. M. Yantosca, B. N. Duncan, and G. W. Sachse (2003), Transport pathways for Asian pollution outflow over the Pacific: Interannual and seasonal variations, *J. Geophys. Res.*, *108*(D20), 8786, doi:10.1029/2002JD003102.

Miyazaki, Y., et al. (2003), Synoptic-scale transport of reactive nitrogen over the western Pacific in spring, *J. Geophys. Res.*, *108*(D20), 8788, doi:10.1029/2002JD003248.

Olivier, J. G. J., A. F. Bouwmann, C. W. M. Van der Maas, J. J. M. Berdowski, C. Veldt, J. P. J. Bloos, A. J. H. Visschedijk, P. Y. J. Zandveld, and J. L. Haverlag (1996), Description of EDGAR version 2.0: A set of global emission inventories of greenhouse gases and zone-depleting substance for all anthropogenic and most natural sources on a per country basis and on $1° \times 1°$ grid, *Rep. 77106002*, Natl. Inst. of Public Health and the Environ., Bilthoven, Netherlands.

Palmer, P. I., D. J. Jacob, D. B. A. Jones, C. L. Heald, R. M. Yantosca, J. A. Logan, G. W. Sachse, and D. G. Streets (2003a), Inverting for emissions of carbon monoxide from Asia using aircraft observations over the western Pacific, *J. Geophys. Res.*, *108*(D21), 8828, doi:10.1029/2003JD003397.

Palmer, P. I., D. J. Jacob, L. J. Mickley, D. R. Blake, G. W. Sachse, H. E. Fuelberg, and C. M. Kiley (2003b), Eastern Asian emissions of anthropogenic halocarbons deduced from aircraft concentration data, *J. Geophys. Res.*, *108*(D24), 4753, doi:10.1029/2003JD003591.

Pan, L., J. C. Gille, D. P. Edwards, P. L. Bailey, and C. D. Rodgers (1998), Retrieval of tropospheric carbon monoxide for the MOPITT experiment, *J. Geophys. Res.*, *103*, 32,277–32,290.

Parish, D. F., and J. C. Derber (1992), The National Meteorological Center's spectral statistical interpolation analysis system, *Mon. Weather Rev.*, *120*, 1747–1763.

Pétron, G., C. Granier, B. Khattatov, J. Lamarque, V. Yudin, J. Müller, and J. Gille (2002), Inverse modeling of carbon monoxide surface emissions using Climate Monitoring and Diagnostics Laboratory network observations, *J. Geophys. Res.*, *107*(D24), 4761, doi:10.1029/2001JD001305.

Peylin, P., P. Bousquet, and P. Ciais (2001), Response technical comment: Inverse modeling of atmospheric carbon dioxide fluxes, *Science*, *294*, 259.

Peylin, P., D. Baker, J. Sarmiento, P. Ciais, and P. Bousquet (2002), Influence of transport uncertainty on annual mean and seasonal inversions of atmospheric CO_2 data, *J. Geophys. Res.*, *107*(D19), 4385, doi:10.1029/2001JD000857.

Prinn, R. G., et al. (2001), Evidence for substantial variation of atmospheric hydroxyl radicals in the past two decades, *Science*, *292*, 1882–1888.

Rodgers, C. D., (2000), *Inverse Methods for Atmospheric Sounding*, World Sci., Tokyo.

Sachse, G. W., G. F. Hill, L. O. Wade, and M. G. Perry (1987), Fast-response, high-precision carbon-monoxide sensor using a tunable diode-laser absorption technique, *J. Geophys. Res.*, *92*, 2071–2081.

Singh, H. B., et al. (2003), In situ measurements of HCN and CH3CN in the Pacific troposphere: Sources, sinks and comparisons with spectroscopic observations, *J. Geophys. Res.*, *108*(D20), 8795, doi:10.1029/2002JD003006.

Streets, D. G., et al. (2003), An inventory of gaseous and primary aerosol emissions in Asia in the year 2000, *J. Geophys. Res.*, *108*(D21), 8809, doi:10.1029/2002JD003093.

Suntharalingam, P., D. J. Jacob, P. I. Palmer, J. A. Logan, R. M. Yantosca, Y. Xiao, M. J. Evans, D. G. Streets, S. L. Vay, and G. W. Sachse (2004), Improved quantification of Chinese carbon fluxes using CO_2/CO correlations in Asian outflow, *J. Geophys. Res.*, *109*, D18S18, doi:10.1029/2003JD004362.

Van der Werf, G. R., J. T. Randerson, G. J. Collatz, and L. Giglio (2003), Carbon emissions from fires in tropical and subtropical ecosystems, *Global Change Biol.*, *9*(4), 547–562.

Wang, J., J. C. Gille, P. L. Bailey, J. R. Drummond, and L. Pan (1999), Instrument sensitivity and error analysis for the remote sensing of tropospheric carbon monoxide by MOPITT, *J. Atmos. Oceanic Technol.*, *16*, 465–474.

Woo, J., et al. (2003), Contribution of biomass and biofuel emissions to trace gas distributions in Asia during the TRACE-P experiment, *J. Geophys. Res.*, *108*(D21), 8812, doi:10.1029/2002JD003200.

Xiao, Y., D. J. Jacob, J. S. Wang, J. A. Logan, P. I. Palmer, P. Suntharalingam, R. M. Yantosca, G. W. Sachse, D. R. Blake, and D. G. Streets (2004), Constraints on Asian and European sources of methane from CH_4-C_2H_6-CO correlations in Asian outflow, *J. Geophys. Res.*, *109*, D15S16, doi:10.1029/2003JD004475.

Yevich, R., and J. A. Logan (2003), An assessment of biofuel use and burning of agricultural waste in the developing world, *Global Biogeochem. Cycles*, *17*(4), 1095, doi:10.1029/2002GB001952.

————————

J. C. Gille, National Center of Atmospheric Research, Boulder, CO 80303, USA.

C. L. Heald, D. J. Jacob, J. A. Logan, and P. I. Palmer, Department of Earth and Planetary Sciences and Division of Engineering and Applied Sciences, Harvard University, Cambridge, MA 02138, USA. (heald@fas.harvard.edu)

R. N. Hoffman and T. Nehrkorn, AER Inc., Lexington, MA 02173, USA.

D. B. A. Jones, Department of Physics, University of Toronto, 60 St. George Street, Toronto, Ontario, Canada M5S 1A7.

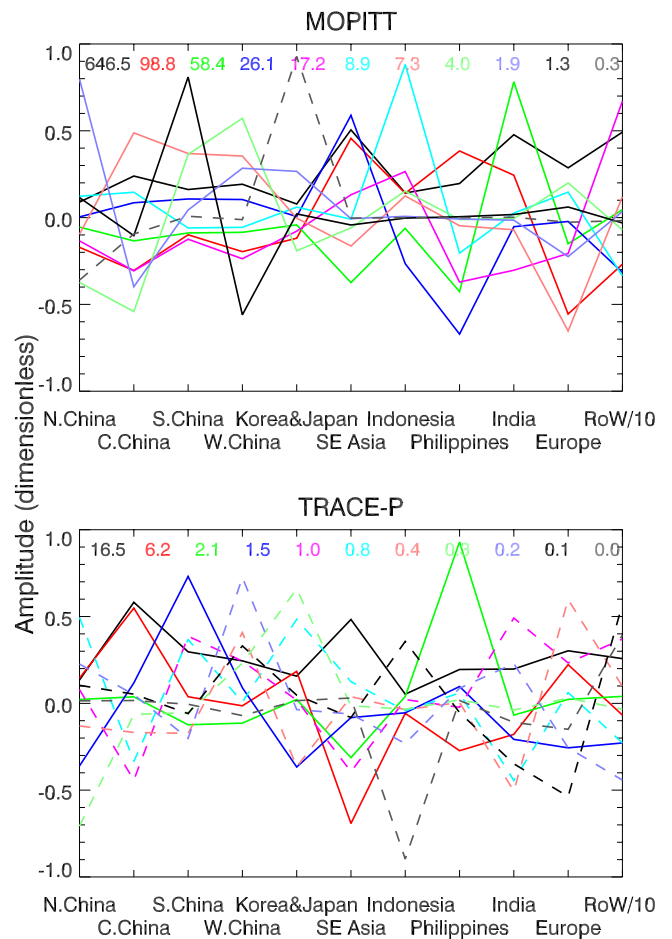G. W. Sachse, NASA Langley Research Center, Hampton, VA 23681, USA.

D. G. Streets, Argonne National Laboratory, Argonne, IL 60439, USA.
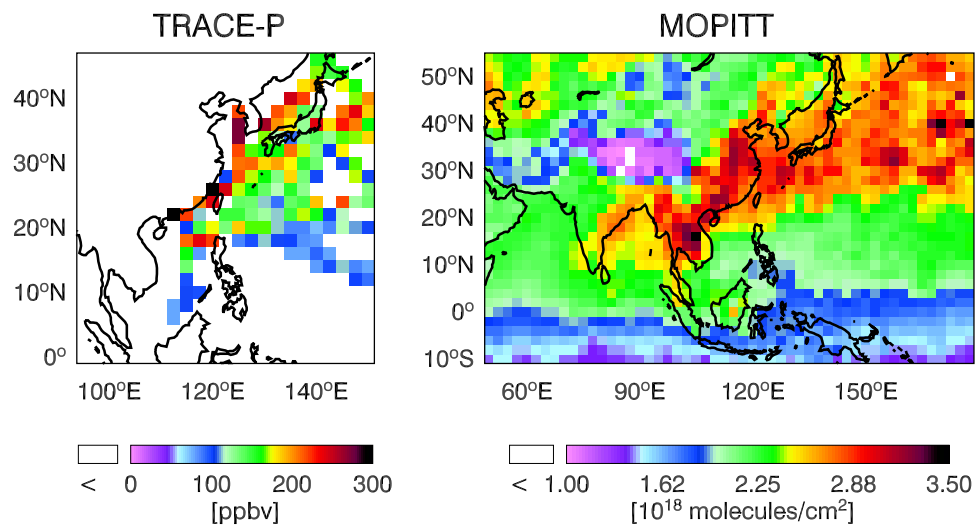
Figure 2. Mean CO observations during the TRACE-P mission (26 February to 9 April 2001) averaged over the 2° × 2.5° grid of the GEOS-CHEM CTM. TRACE-P aircraft concentrations averaged over all altitudes are shown on the left. The MOPITT CO columns (morning overpasses only) are shown on the right.
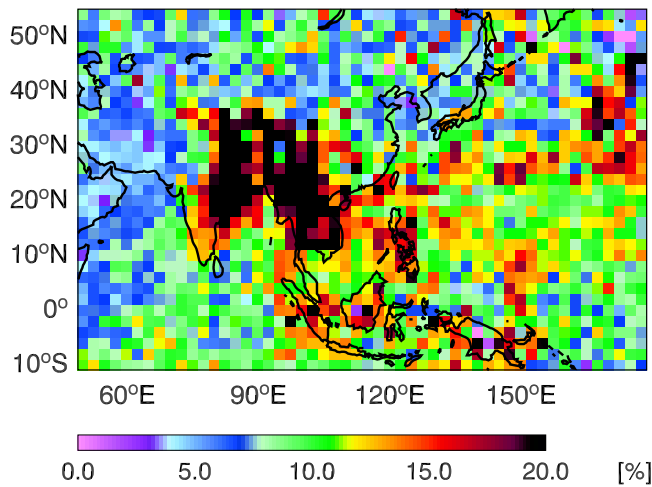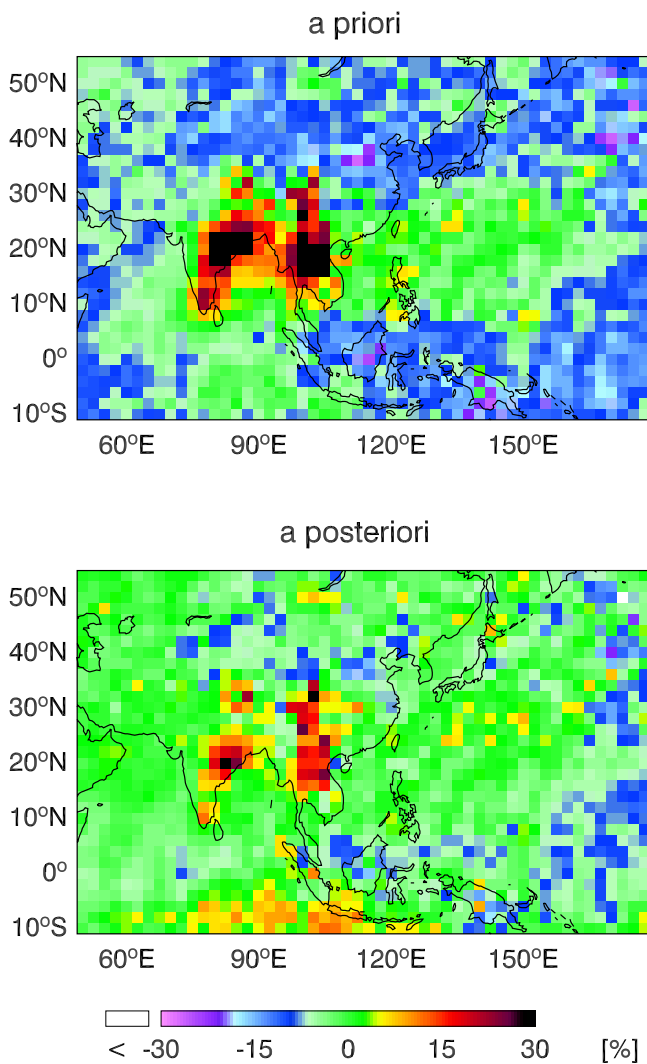
Figure 4. Total observational error variance (diagonal elements of $\mathbf{S}_\Sigma$) for the MOPITT data using GEOS-CHEM as forward model (morning overpasses only).
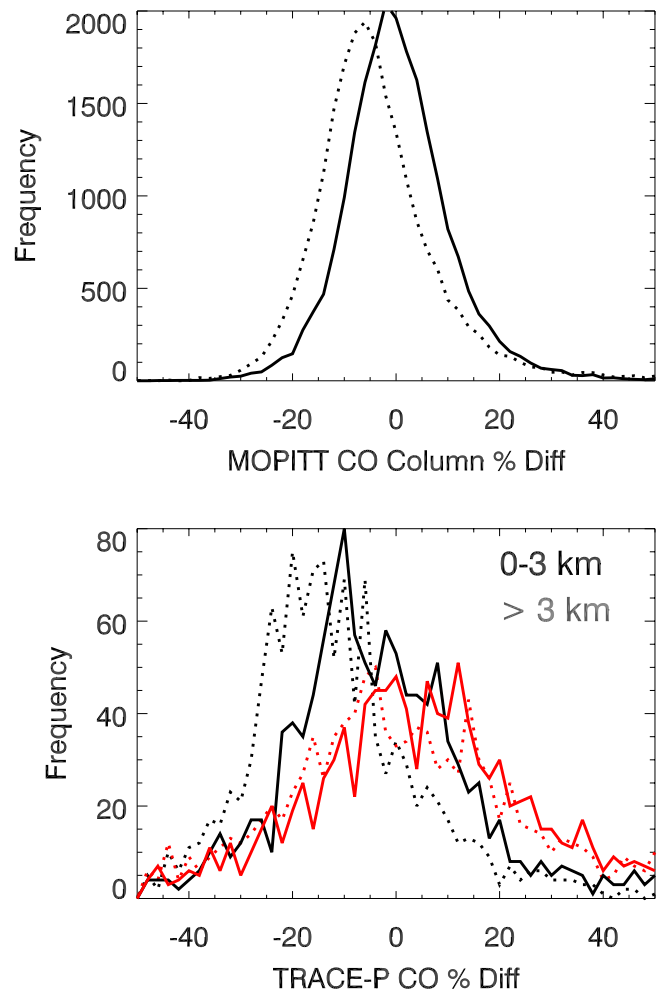

Figure 5. Singular vectors of the prewhitened Jacobian $\tilde{\mathbf{K}}$ matrix for the 11-element state vector given in Table 1 for (top) the MOPITT observations and (bottom) the aircraft observations. Each line represents one singular vector. As an example: the vector corresponding to the green solid line for the TRACE-P observations includes strong signatures for sources in the Philippines and SE Asia. The singular values corresponding to each vector are shown at the top of the figure. The singular vectors which cannot be retrieved above the noise in the system are indicated by the dotted lines.
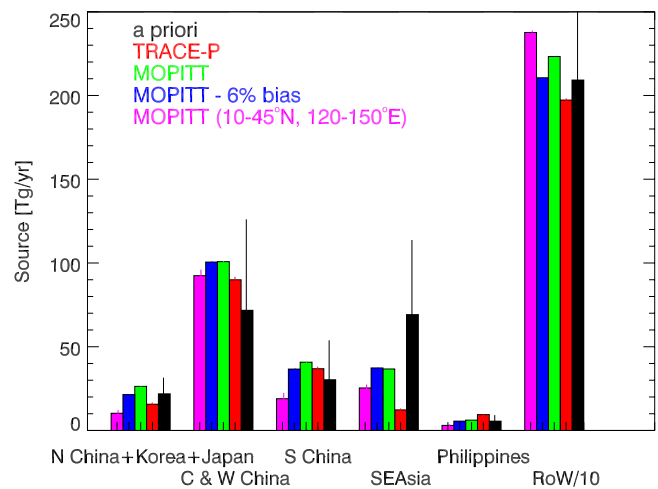
Figure 8. GEOS-CHEM model bias in the simulation of MOPITT observations when either the a priori or the best case a posteriori CO sources (Table 1) are used as input to the model. Bias is defined as the mean of the difference between simulated and observed concentrations averaged over the spring 2001 observing period. Color scale is saturated at 30% but model bias in the a priori comparison ranges up to 75% over SE Asia.

Figure 9. GEOS-CHEM model bias in the simulation of (top) MOPITT observations or (bottom) TRACE-P observations when either the a priori (dotted) or the best case a posteriori (thick) CO sources (Table 1) are used as input to the model. Bias is defined as the mean of the difference between simulated and observed concentrations averaged over the spring 2001 observing period.
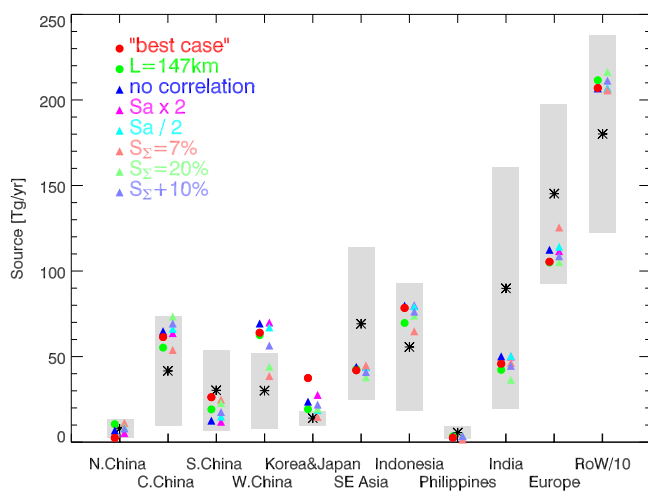
Figure 10. Sensitivity of the a posteriori CO source estimates to the error characterization for the MOPITT observation system. Results from a number of sensitivity test cases with modified error assumptions (cases 4–10 of Table 2) are shown together with the best case. Stars and shaded gray bars indicate a priori estimates and uncertainties.

Figure 13. Comparison of a posteriori source estimates for CO as constrained by the aircraft and MOPITT observations using a state vector containing only the six regions identified in the figure (test cases 18–21). Included are results for MOPITT corrected by its 6% positive column bias, and for MOPITT sampled over the TRACE-P flight region only (10–45°N, 120–150°E).